POLARIZATION, PLEASE

--- *THE MISSING TOOL OF THE TRADE*

Wen-Ping **CHEN** 陳文屏

National Central University

2023.11.20 兩岸天文望遠鏡會議

Outline

- Cosmic Polarization
- Imaging Polarimeter TRIPOL at Lulin

✓ Young Stellar Environments

✓ Magnetically Active Stars

Cosmic Polarization in a nutshell

Monochromatic linear/circular/elliptical polarization

Stokes parameters: I, Q, U, V

$I > 0$; Q, U, V any

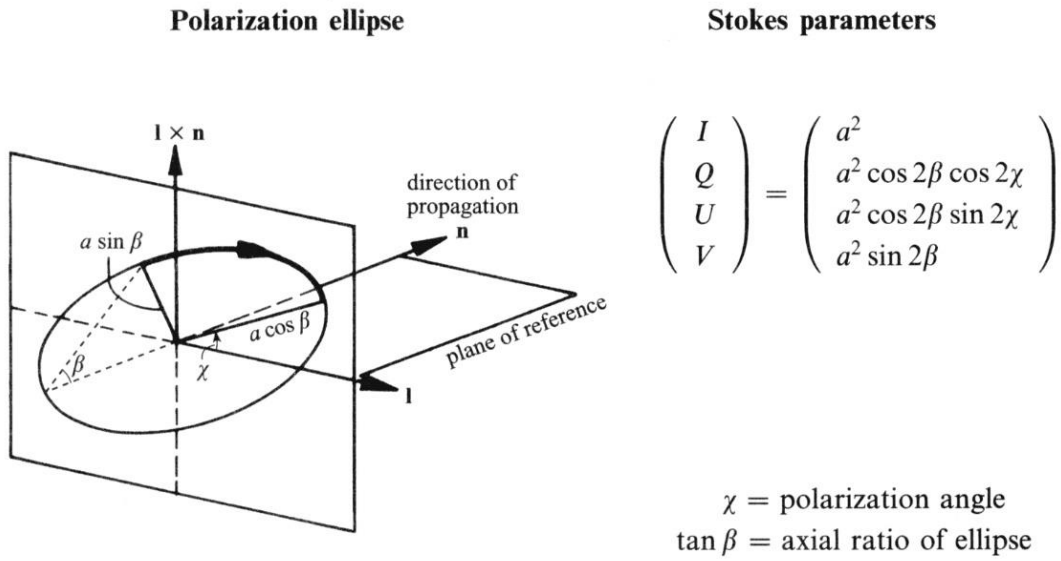

Possible Mechanisms

- Synchrotron emission
- Scattering
  (*Thomson, Rayleigh, Mie*)
- Index of refraction

For linear polarization, $\sin 2\beta = 0$
$\rightarrow V = 0$, $Q = a^2 \cos 2\chi$, $U = a^2 \sin 2\chi$,
a: amplitude, χ: polarization angle.

Polarization ← asymmetric configuration

- ✓ Source itself
- ✓ Medium in between (scattering geometry; $\vec{B}$)

λ	Source	P_{max} (%)
γ rays	Pulsars (expected)	100
X rays	Solar flares	5
	AGNs	20
Optical	Dust on starlight (linear)	10
	Sunspots	100
	Symbiotic stars (Raman)	10
	Reflection nebulae (HH)	60
	Crab, blazars (synchrotron)	50

λ	Source	P_{max} (%)
IR/smm	Scattering by large grains	75
	Dust emission	2
Radio	Quasars	70
	OH masers	100
	Zeeman (21 cm, 18 cm) absorption	2
	Solar flares, flare stars	**10 – 100**
	Extragalactic jets	50
	Cosmic microwave background	<0.01

From Tinbergen

Polarization by Reflection

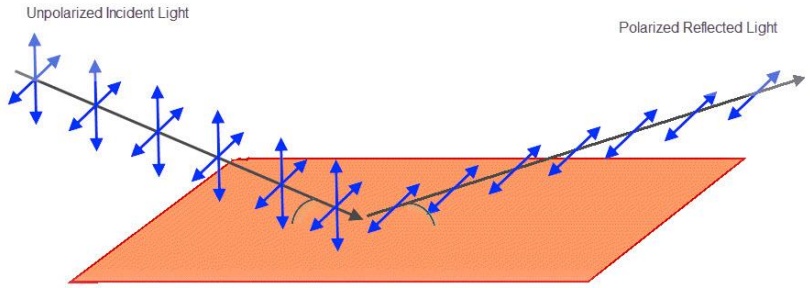

... induced and
radiates like a dipole

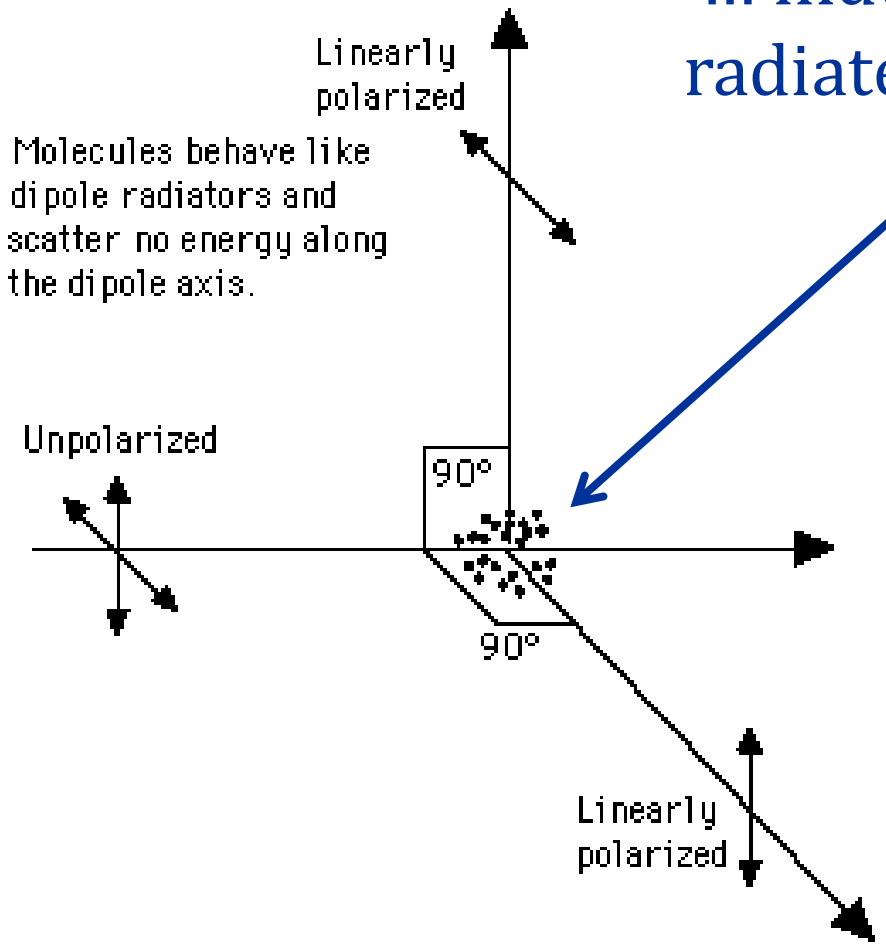

hyperphysics

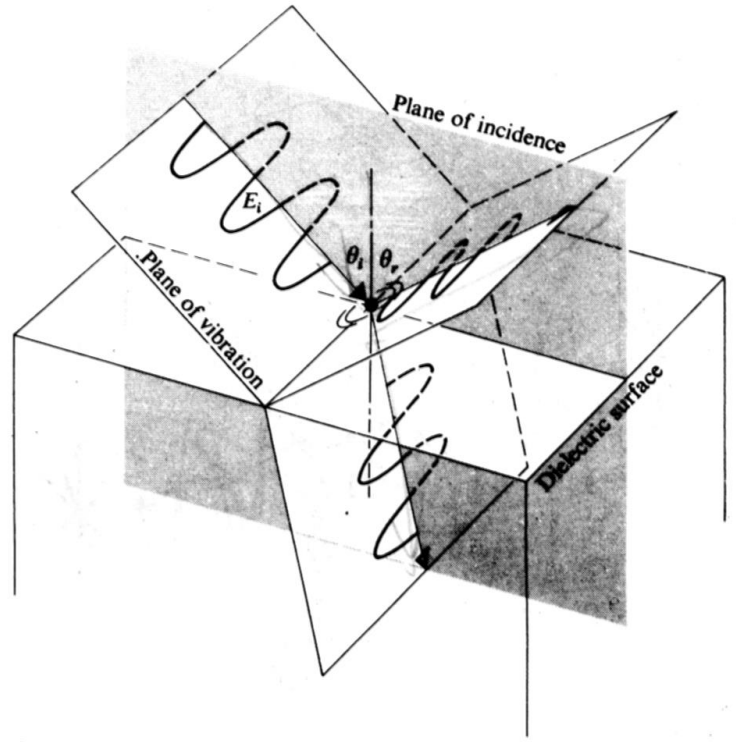

Fig. 8.40 A wave reflecting and refracting at an interface.

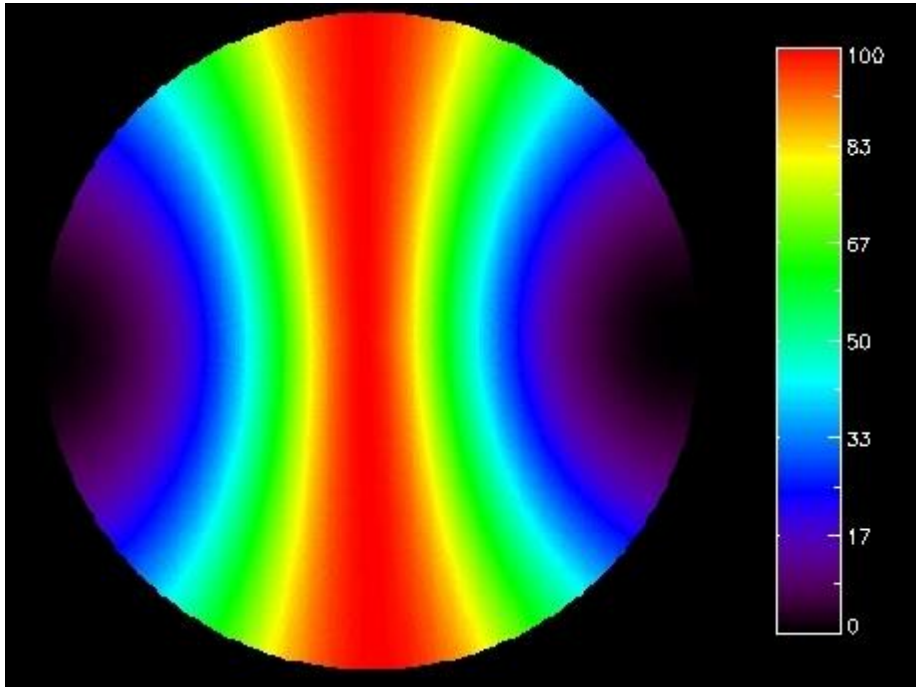

The Rayleigh sky at sunset or sunrise
http://en.wikipedia.org/wiki/Rayleigh_sky_model

Rayleigh Scattering

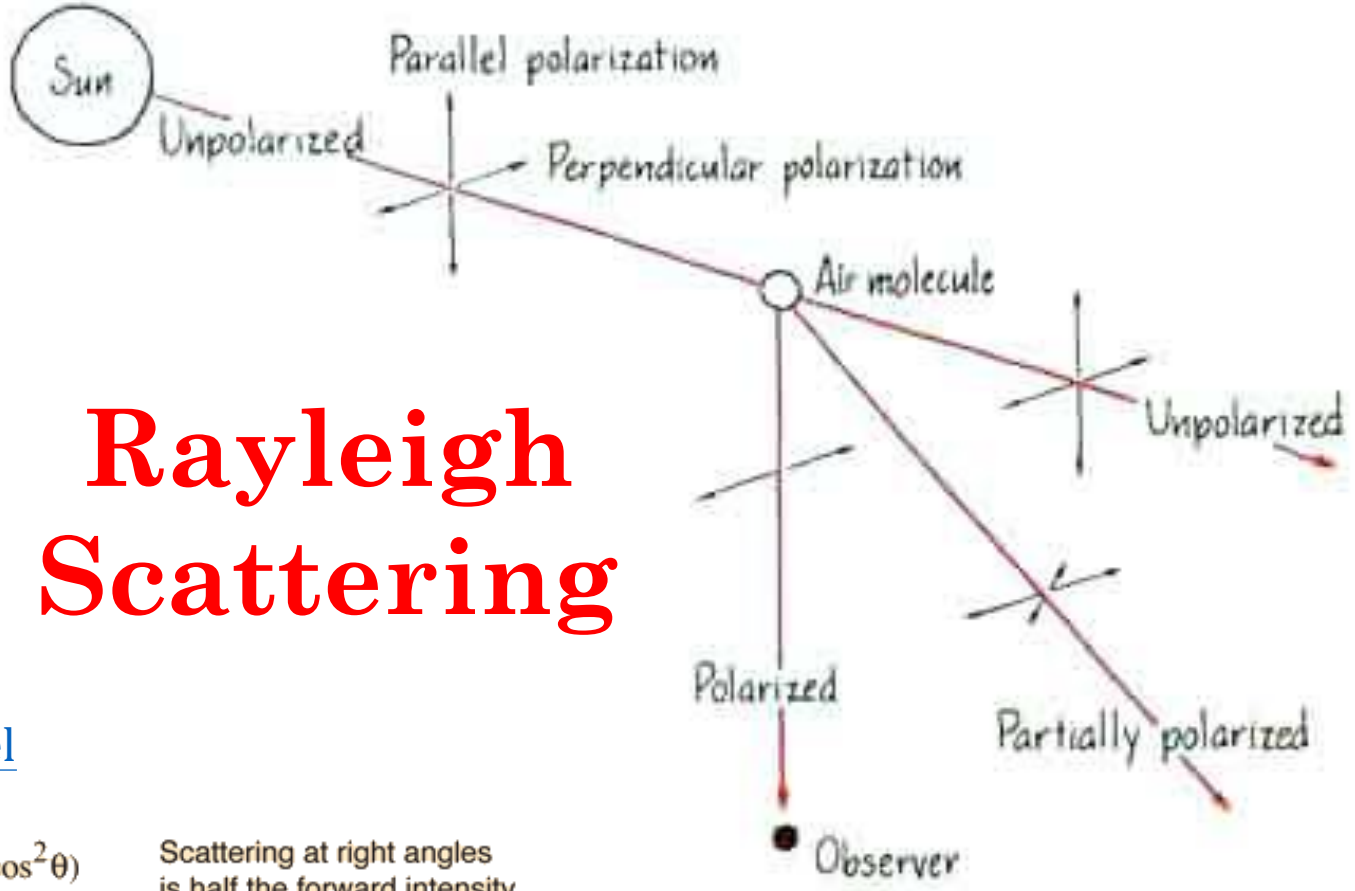

$$I = I_0 \frac{8\pi^4 N\alpha^2}{\lambda^4 R^2}(1 + \cos^2\theta)$$

Scattering at right angles is half the forward intensity for Rayleigh scattering

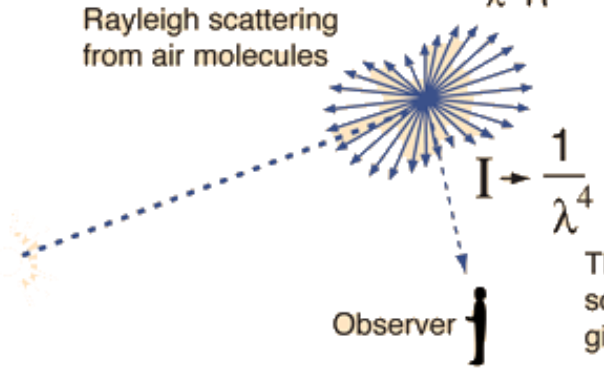

$$I \to \frac{1}{\lambda^4}$$

N = # of scatterers
α = polarizability
R = distance from scatterer

The strong wavelength dependence of Rayleigh scattering enhances the short wavelengths, giving us the blue sky.

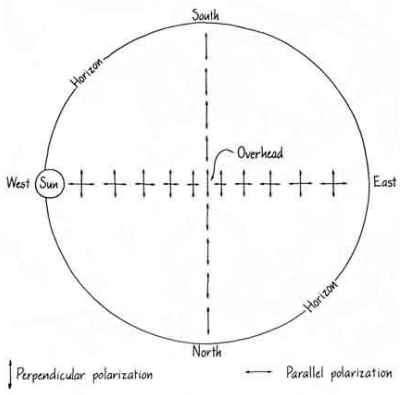

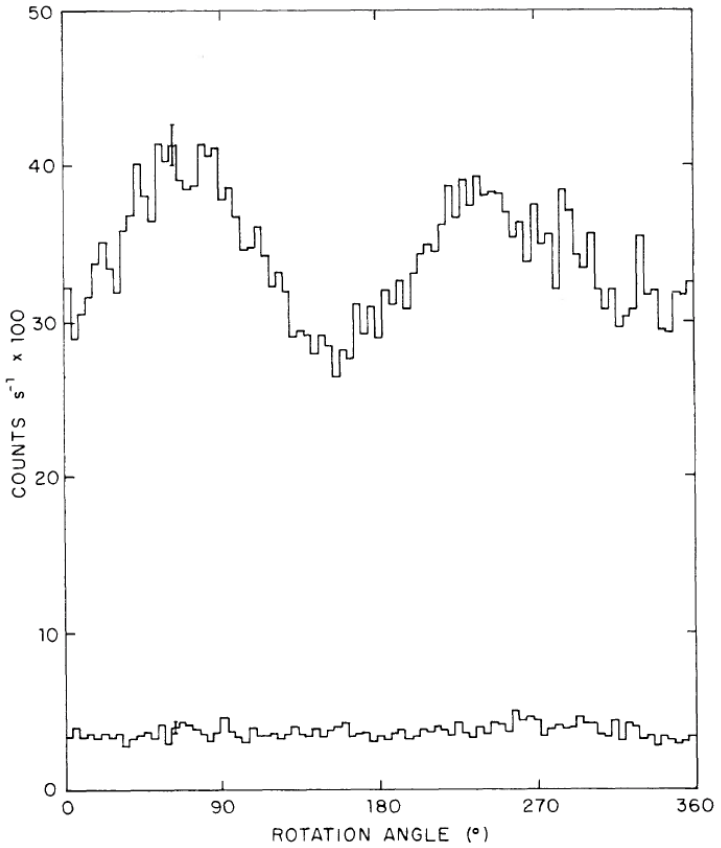

X-ray linear polarization of the Crab Nebula (top) and of the background (bottom) at 4.77 Å (2.6 keV), from Weisskopf et al. (1978).

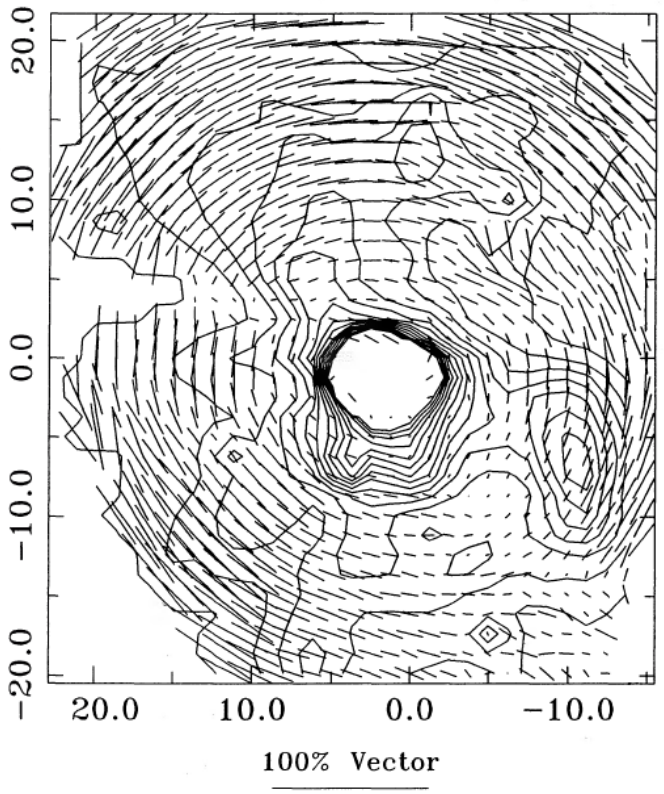

The *K*-band polarization vector map of the embedded S106/IRS 4 (0, 0) showing scattering polarization, from Aspin et al. (1990).

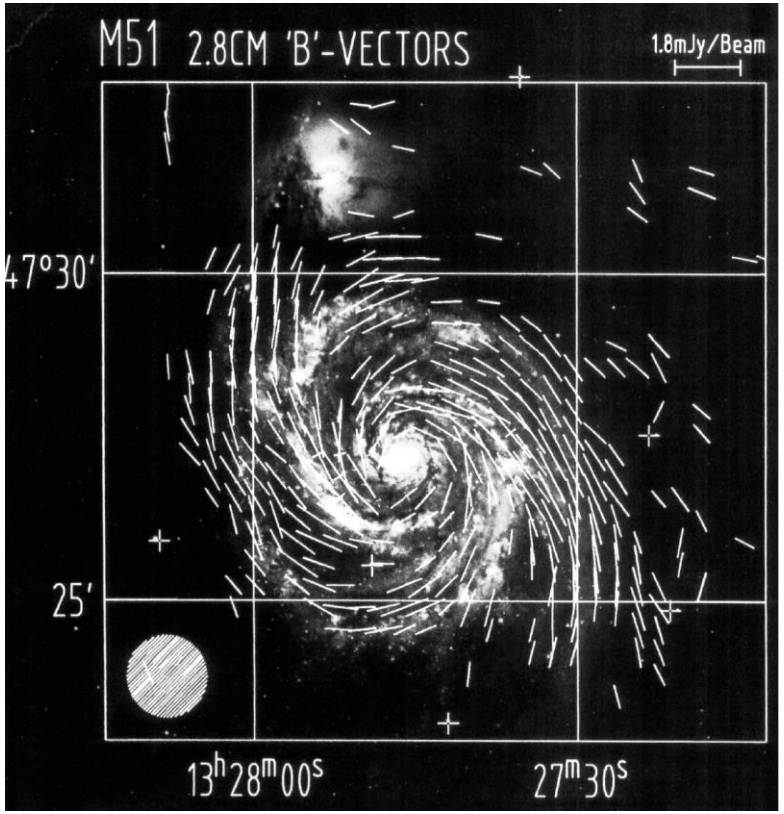

Magnetic field structure of M51, as derived by polarimetry at 2.8 cm due to synchrotron radiation, from Aspin et al. (1990).

Interstellar Polarization of the Milky Way

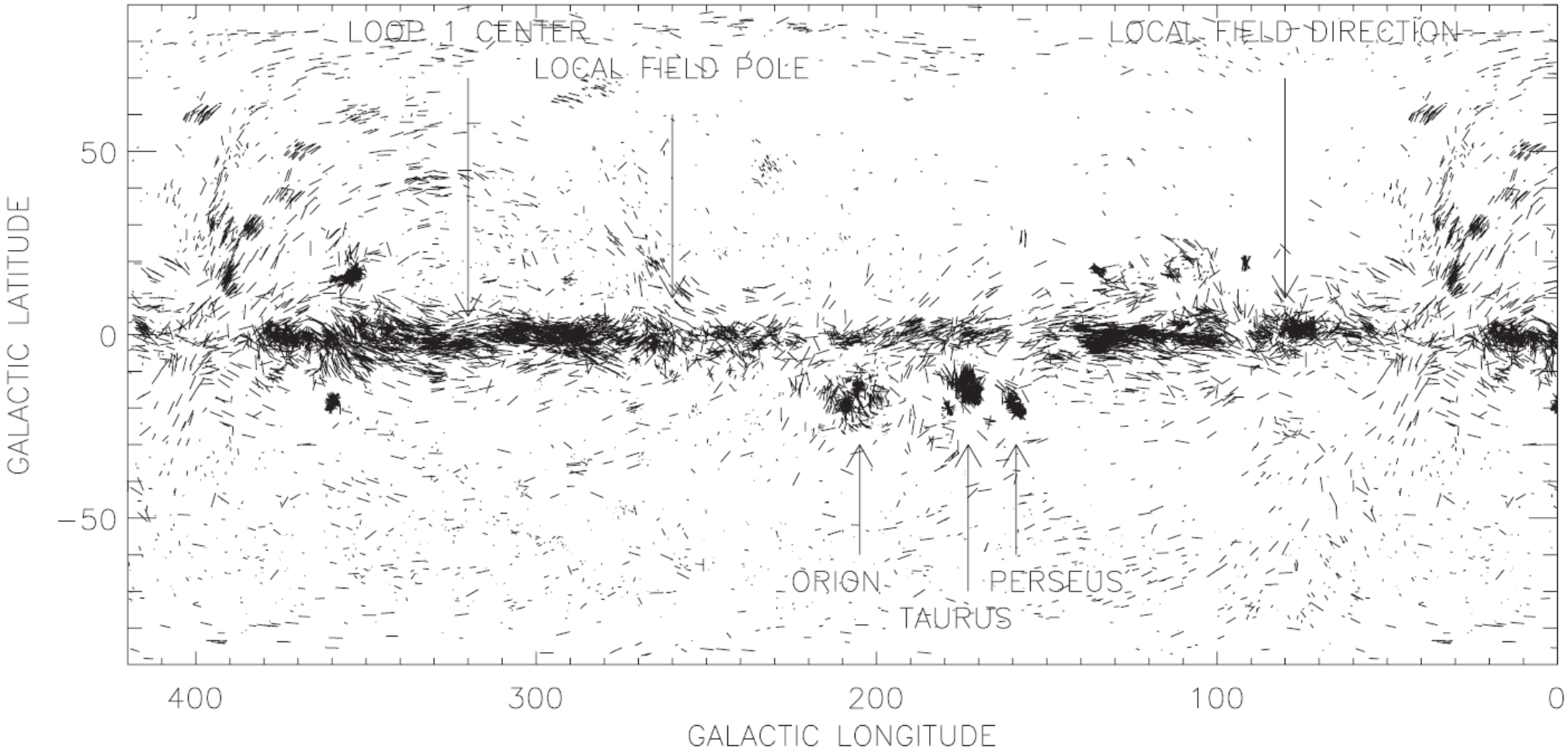

Fig. 1. Starlight polarization of 8662 stars. The orientation of each star's polarization is indicated by a short line whose length L in great-circle degrees is $L = [4 < 2P]°$, where P is the percentage polarization; for L, we plot whichever of the two quantities is smaller

Heiles & Crutcher (2005)

Dichroism of the ISM

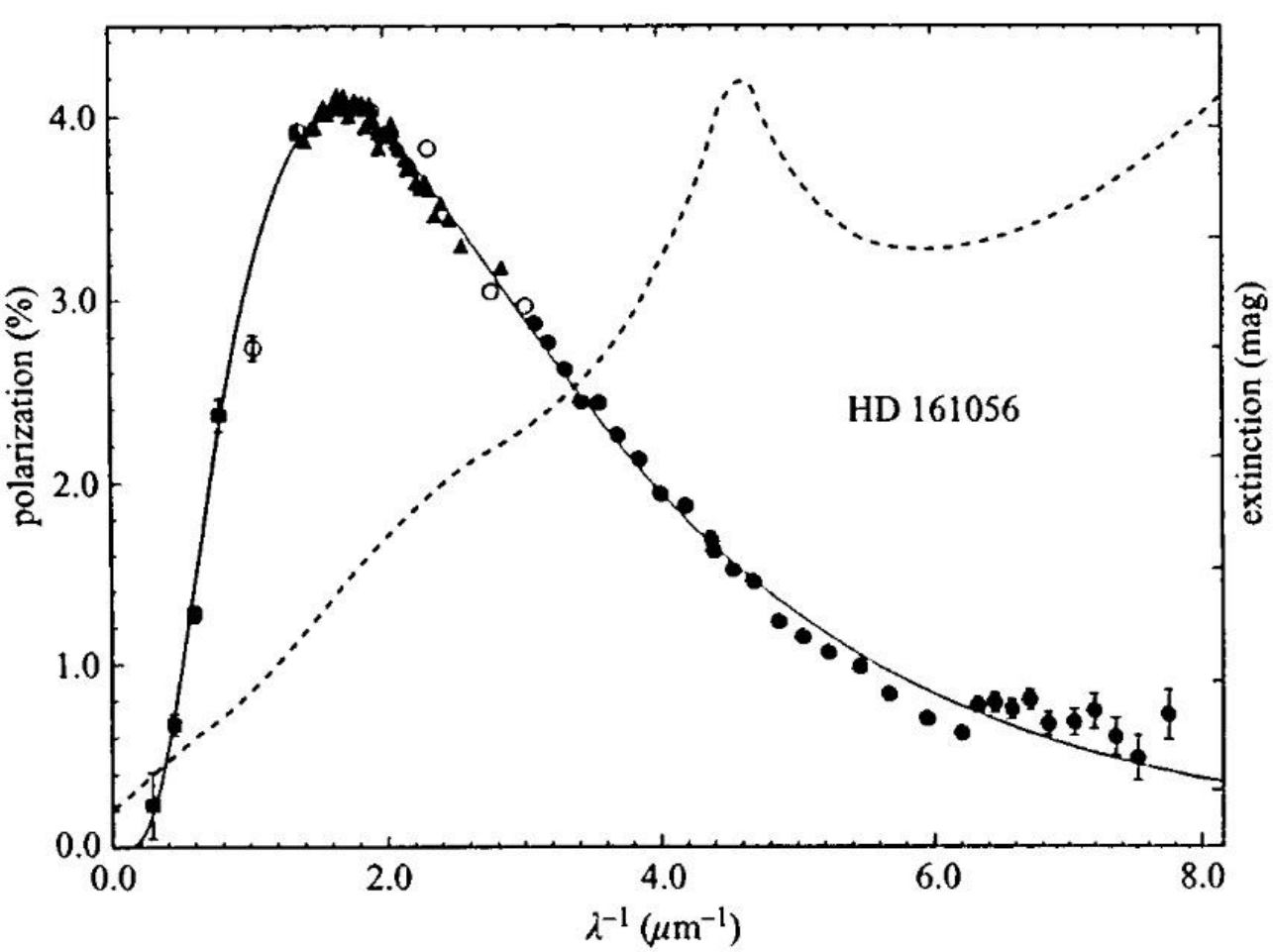

Tinbergen

Polarization peaks at a wavelength related to the average size of the IS grains (“Serkowski law”)

A thermalized ISM elongated grain tends to spin along its minor axis: $\vec{\omega} \longrightarrow \vec{B}$

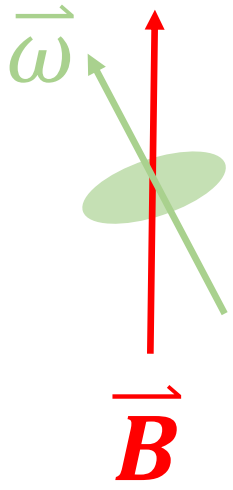

Davis-Greenstein alignment mechanism --- paramagnetic dissipation

http://bgandersson.net/grain-alignment

Observations in OIR $\vec{P} \parallel \vec{B}$

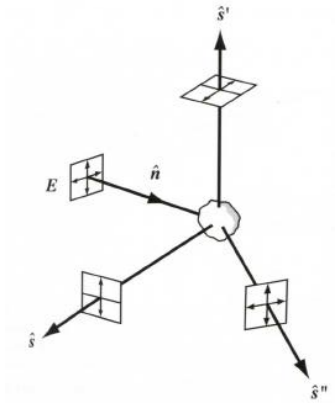

Stahler & Pallo 2004

Scattering by dust

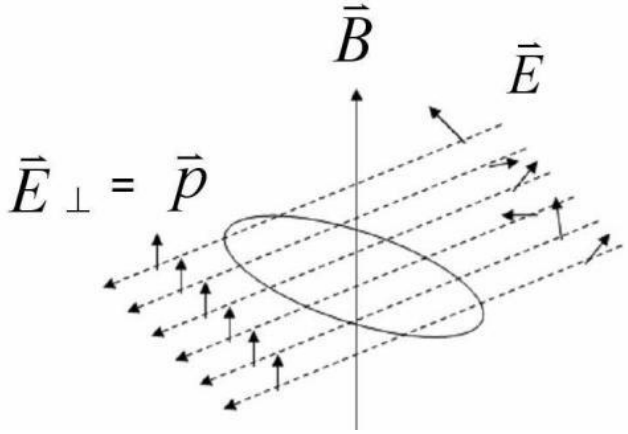

Dichroic extinction by aligned dust

Observations in FIR to mm $\vec{P} \perp \vec{B}$

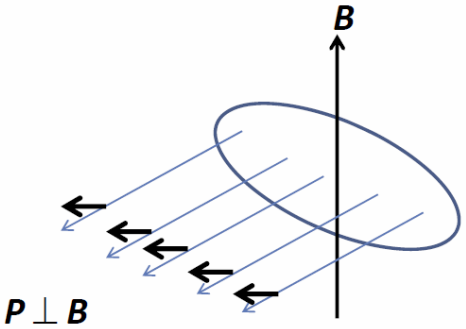

*Polarized thermal emission by dust aligned by **B***

Courtesy: Tamura

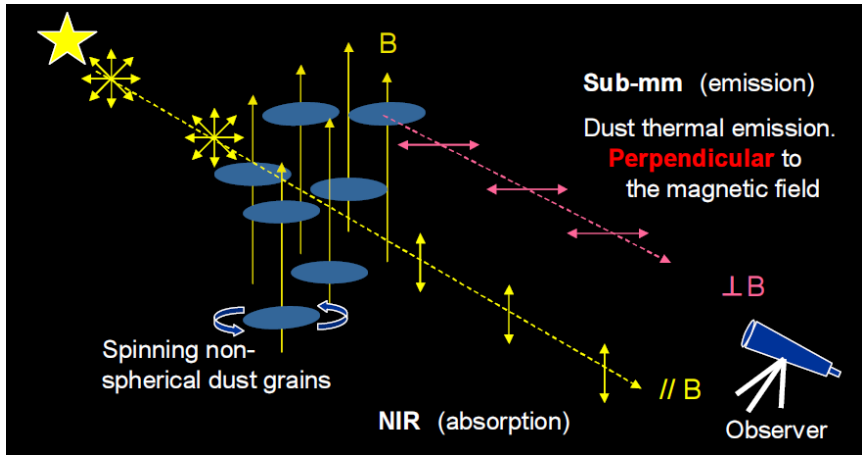

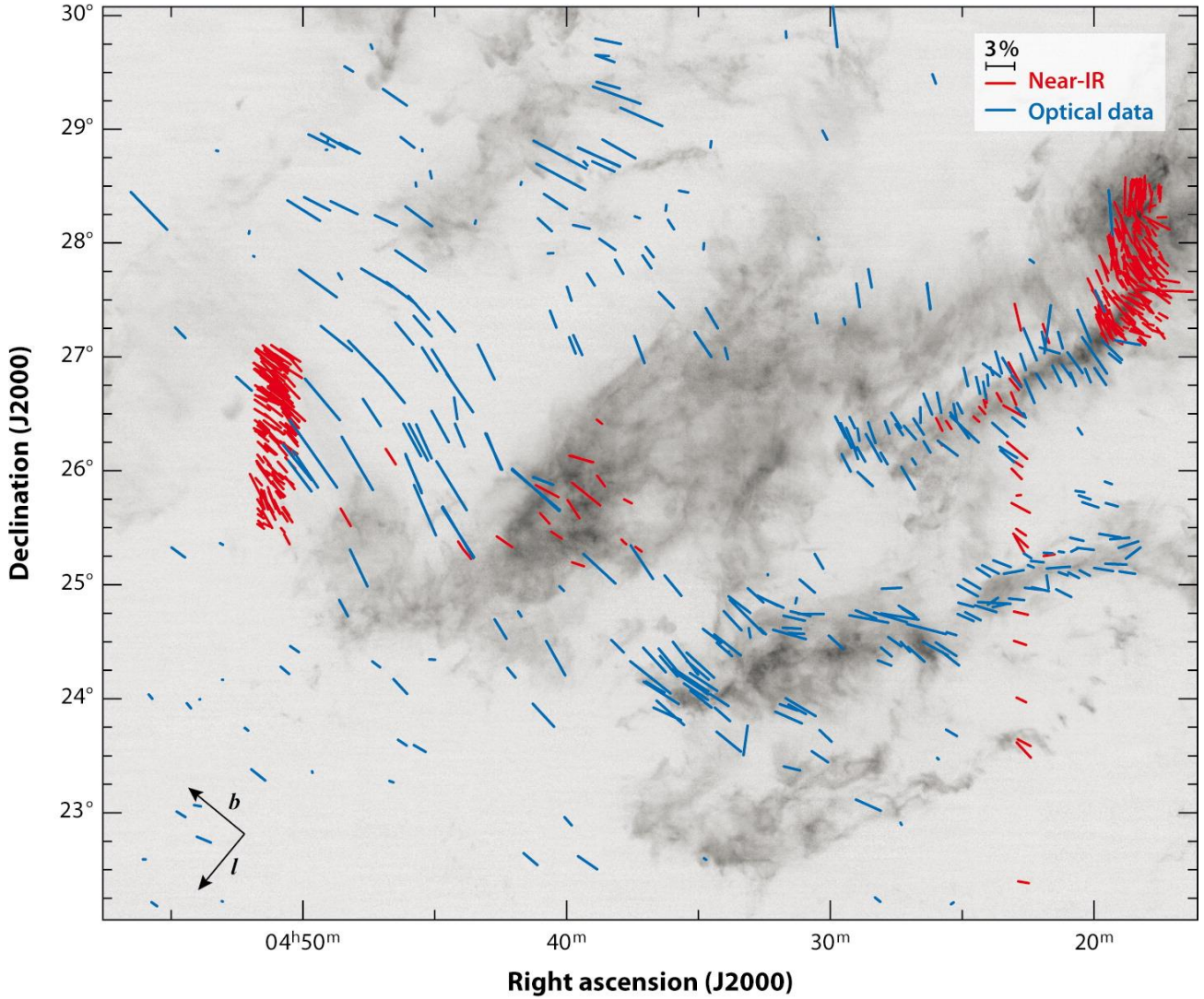

Crutcher RM. 2012.
Annu. Rev. Astron. Astrophys. 50:29–63

Organized magnetic field morphology in the Taurus dark-cloud complex superposed on a ^{13}CO map (Chapman et al. 2011). Blue lines show polarization measured at optical wavelengths and red lines show near-IR (*H*-band and *I*-band) polarization.

Dichroic extinction by dust (optical and near-IR)

$$\vec{P} \parallel \vec{B}$$

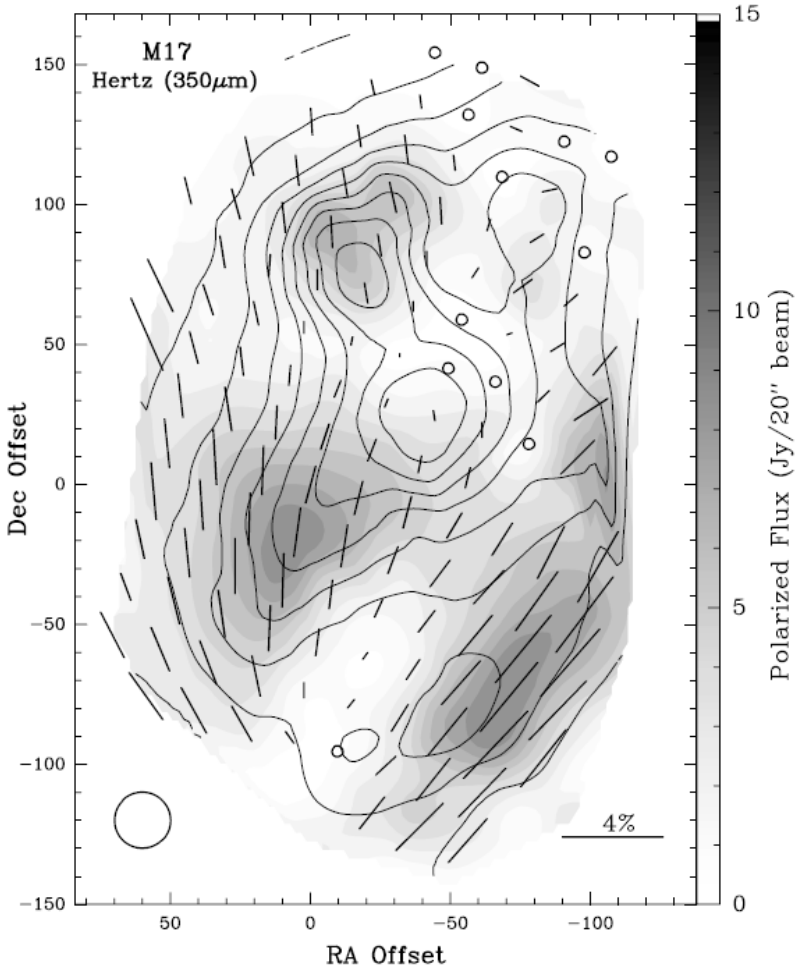

FIG. 6.—HERTZ polarization map of M17 at 350 μm. All of the polarization vectors shown have a polarization level and error such that $P > 3\sigma_P$. Circles indicate cases where $P + 2\sigma_P < 1\%$. The contours delineate the total continuum flux (from 10% to 90% with a maximum flux of ≈700 Jy), whereas the underlying gray scale gives the polarized flux according to the scale on the right. The beam width (≃20″) is shown in the lower left corner and the origin of the map is at R.A. = $18^h17^m31^s.4$, decl. = $-16°14'25''.0$ (B1950.0).

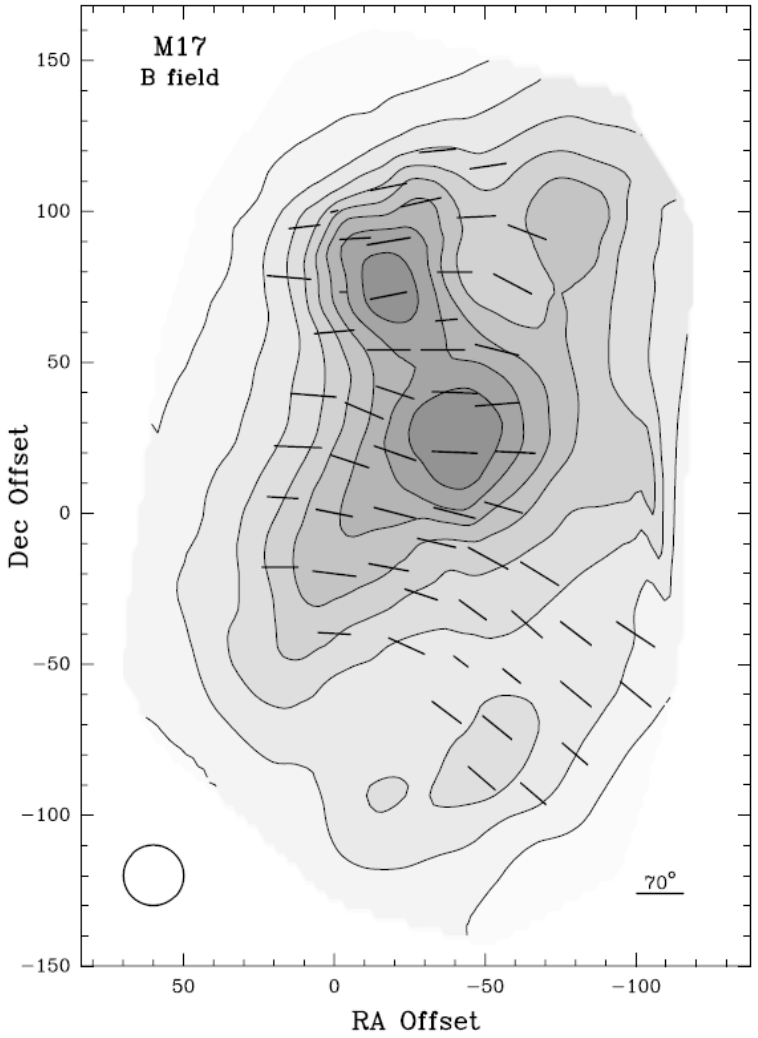

FIG. 11.—Orientation of the magnetic field in M17. The orientation of the projection of the magnetic field in the plane of the sky is shown by the vectors and the viewing angle is given by the length of the vectors (using the scale shown in the bottom right corner). The contours and the gray scale delineate the total continuum flux. The beam width (≃20″) is shown in the lower left corner, and the origin of the map is at R.A. = $18^h17^m31^s.4$, decl. = $-16°14'25''.0$ (B1950.0).

Thermal emission by dust (far-IR, and smm)

$\overrightarrow{P} \perp \overrightarrow{B}$

Houde et al. (2002)

AGNs --- Pol of lines vs continuum

Forbidden lines ~1%; continuum 16% due to electron scattering

→ broad-line vs narrow-line regions of the central BH and the accretion disk

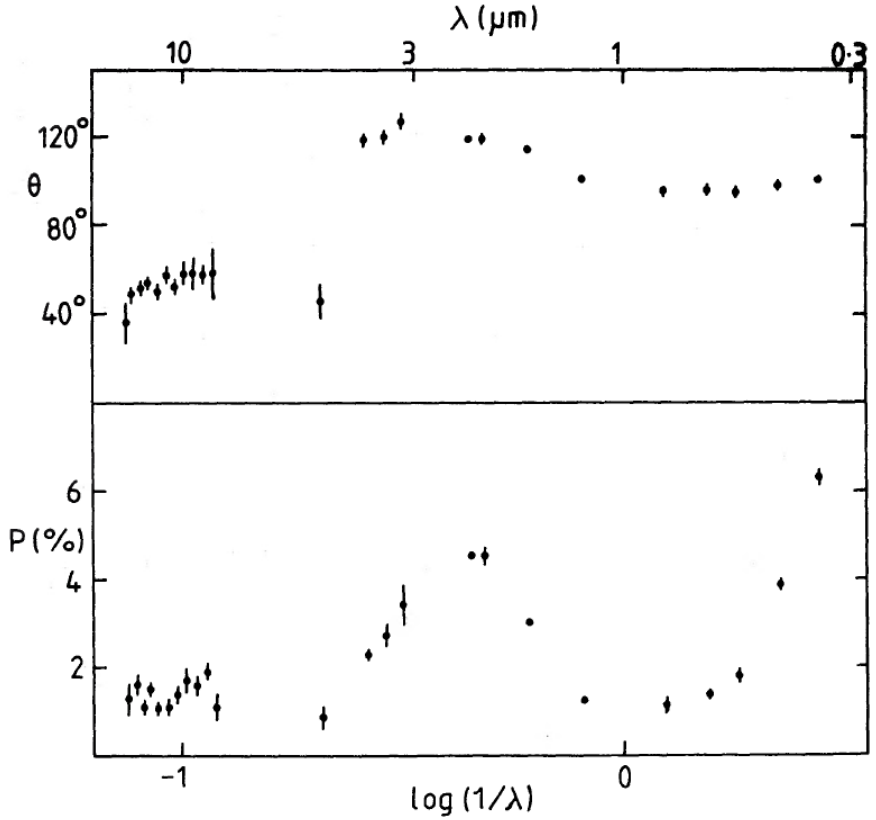

Bailey+88

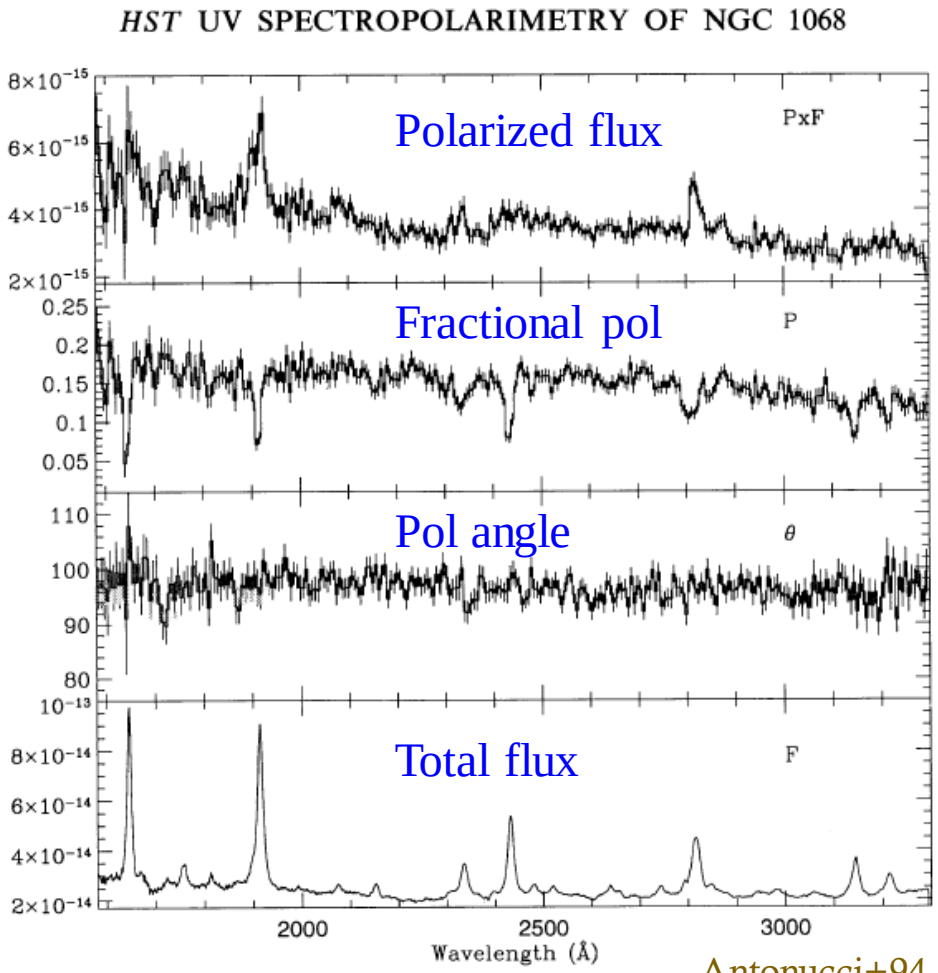

Antonucci+94

ESA Voyage 2050 White Paper

Spectropolarimetry as a Tool for Understanding the Diversity of Planetary Atmospheres

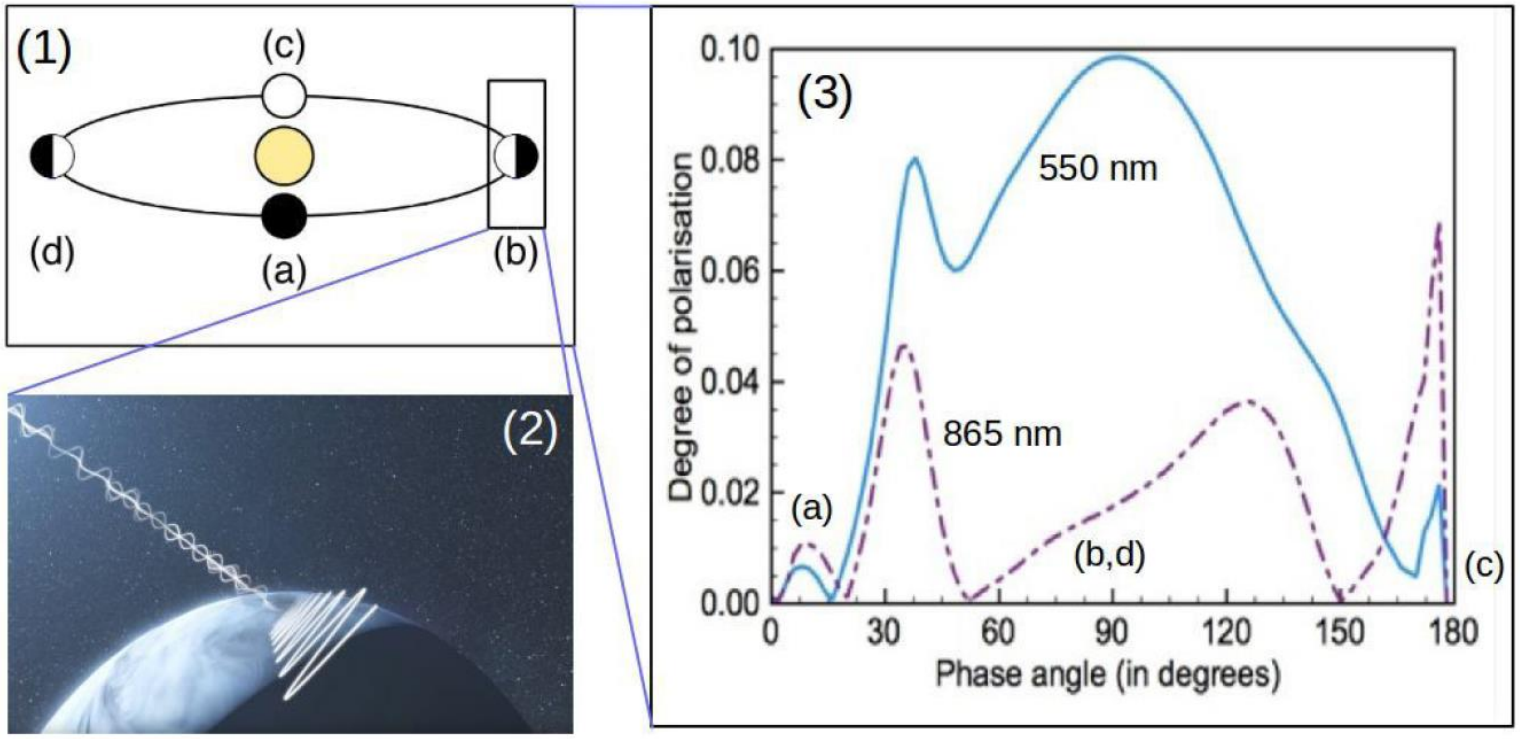

Figure 1. Panels (1) & (2): schematic of a planetary system in which the unpolarized starlight becomes polarized through reflection by a planetary atmosphere. Panel (3): degree of polarization (P; in %) of a cloudy Earth-like planet as a function of planetary orbital phase, labeled as in panel (1). The different lines are for different wavelengths.

Credits: (1) S. Wiktorowicz (2) ESO (3) D. M. Stam.

UV polarimetry, doable only in space, is prolific in studies of exoplanets, stars, ISM, and AGN astrophysics.

ESPaDOnS: an Echelle SpectroPolarimetric Device for the Observation of Stars (on the CFHT)

In a single exposure 370 to 1,050 nm
R=80,000

SPIRou: SPectropolarimètre InfraROUge (on the CFHT)

Fiber-fed IR echelle spectrograph; optimized for RV

In a single exposure 950 to 2350 nm
R=75,000

Lulin Observatory

Lon: 120° 52' 25" E
Lat: 23° 28' 07" N
Alt: 2,862 m
in central Taiwan
limited space
Sky 21.28 mag/sq"
Data: 1,450 hrs/yr

One-Meter (LOT)
(TAOS 50 cm × 4)
SLT 40
LWT40
L35
Experiments of
meteorology, space
and earth sciences

Triple Range Imager and POLarimeter (TRIPOL)

@ Lulin One-meter Telescope (LOT) since 2012

Simple, robust, versatile, & economic, suitable for small telescopes

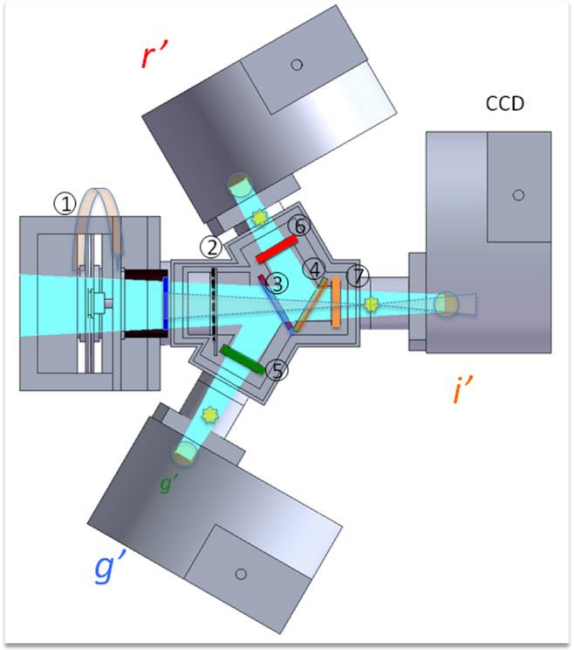

(1) Wave-plate; (2) Wire grid; (3) Dichroic mirror 1; (4) Dichroic mirror 2; (5) g' filter; (6) r' filter; (7) i' filter; (8) CCD camera

♠ Polarization unit

Half wave plate

♥ Color-decomposition unit

Band-pass filters

g'(475nm, 400—500nm)

r'(620nm, 550—680nm)

i'(760nm, 700—830nm)

♦ Data-acquisition unit

♣ Performance

- ✓ FoV ~ 4.7 × 4.7 arcmin^2 with 0.50" pixels
- ✓ Photometry (S/N~10 with 100-s integration)
  - → *g'*~19, *r'*~18.5, *i'*~18 mag
- ✓ Polarimetry > 0.3% weather permitting

Observations and Data analysis

Observing Strategy

1. Aperture photometry at 4 angles
2. 5—10 sets/observation
3. Flux calibration
4. Average the fluxes
   → Stokes parameters
   → polarization and position angle
5. Standard stars (unpolarized/polarized)
   → unpolarized: accuracy ~0.3%
   → pol angle offset (~30°—40°)

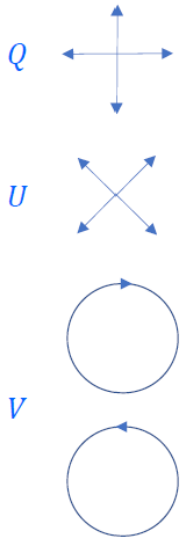

Stokes parameters

$$I = \frac{1}{2}(I_0 + I_{45} + I_{22.5} + I_{67.5})$$

$$Q = I_0 - I_{45}$$

$$U = I_{22.5} - I_{67.5}$$

Polarization and position angle

$$P = \frac{\sqrt{Q^2 + U^2}}{I}$$

$$\theta = 0.5 \arctan(\frac{U}{Q})^{-1}$$

Debias polarization: $P_{db} = \sqrt{P^2 - (\delta P)^2}$ (Wardle & Kronberg 1974)

The Astrophysical Journal, 871:183 (12pp), 2019 February 1 https://doi.org/10.3847/1538-4357/aaf793

Diagnosing the Clumpy Protoplanetary Disk of the UXor Type Young Star GM Cephei

P. C. Huang[1], W. P. Chen[1,2], M. Mugrauer[3], R. Bischoff[3], J. Budaj[4], O. Burkhonov[5], S. Ehgamberdiev[5], R. Errmann[6,7], Z. Garai[4], H. Y. Hsiao[1], C. L. Hu[8], R. Janulis[9], E. L. N. Jensen[10], S. Kiyota[11], K. Kuramoto[12], C. S. Lin[1], H. C. Lin[1], J. Z. Liu[13], O. Lux[3], H. Naito[14], R. Neuhäuser[3], J. Ohlert[15,16], E. Pakštienė[17], T. Pribulla[4], J. K. T. Qvam[18], St. Raetz[19,20], S. Sato[21], M. Schwartz[22], E. Semkov[23], S. Takagi[12], D. Wagner[3], M. Watanabe[24], and Yu Zhang[13]

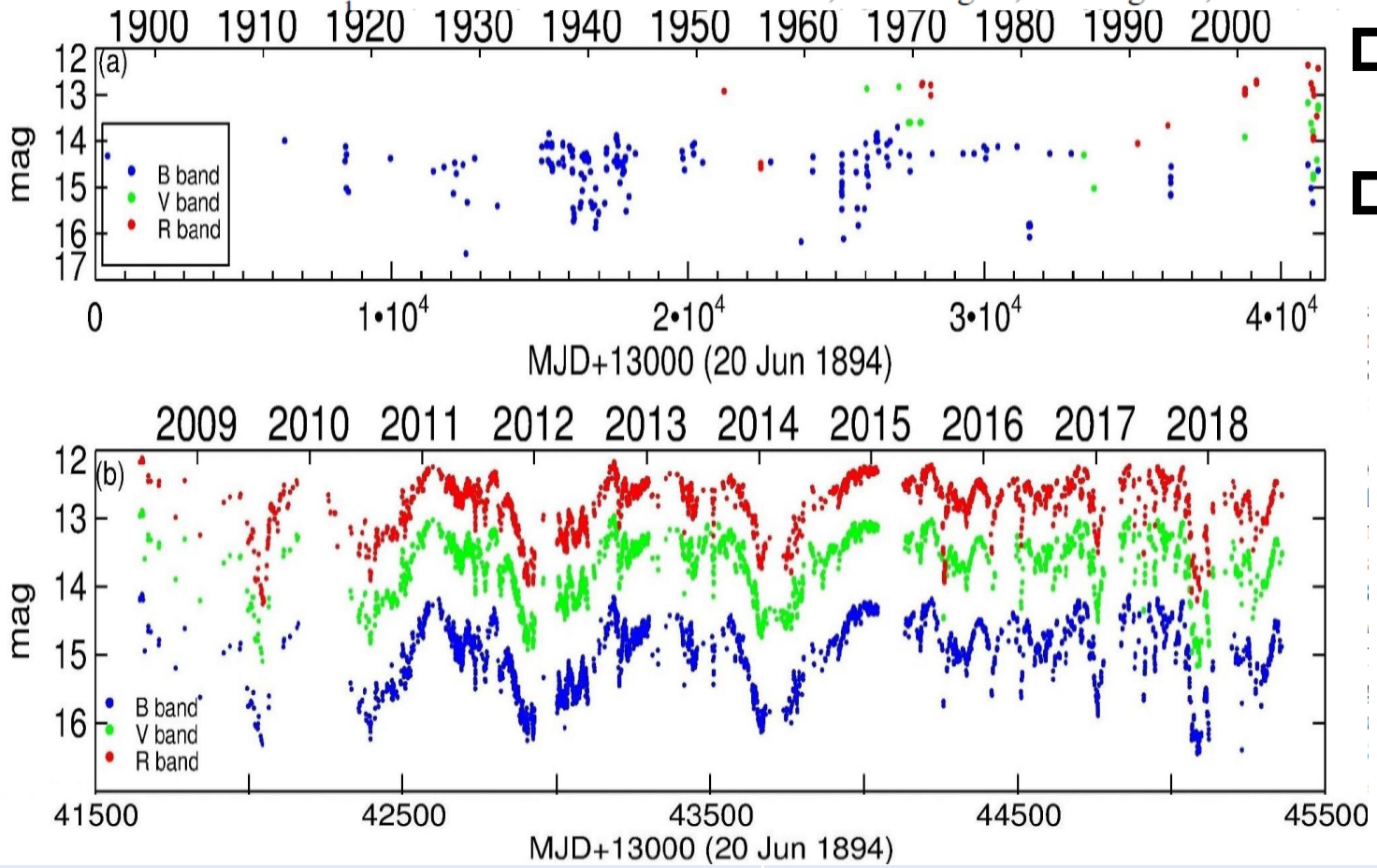

- Short events → depth ∝ duration
  → A_V ~ 1 mag / 30 days
- Long events → A_V ≈ 1.5 mag
  → string or spiral arm?

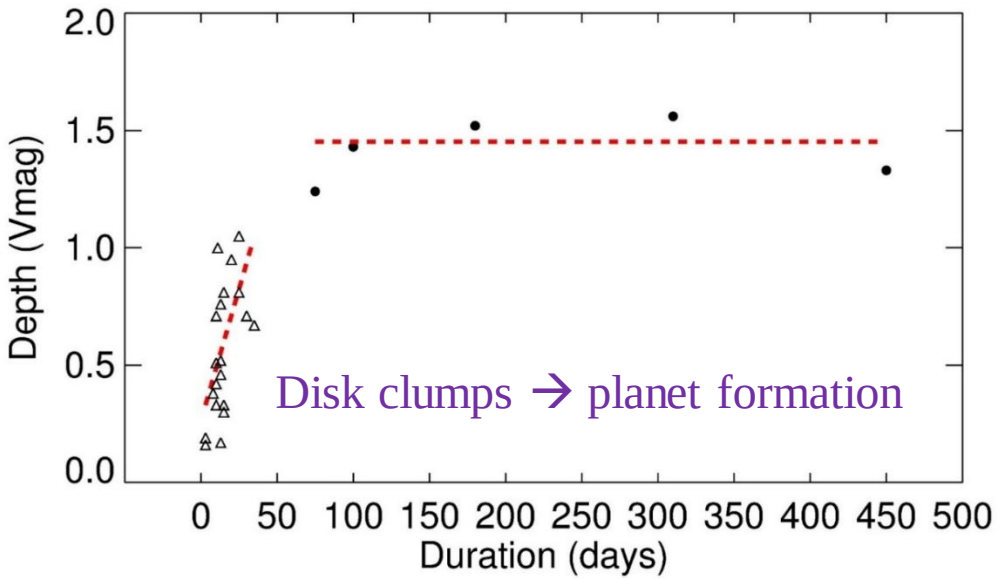

Polarized vs Unpolarized Light

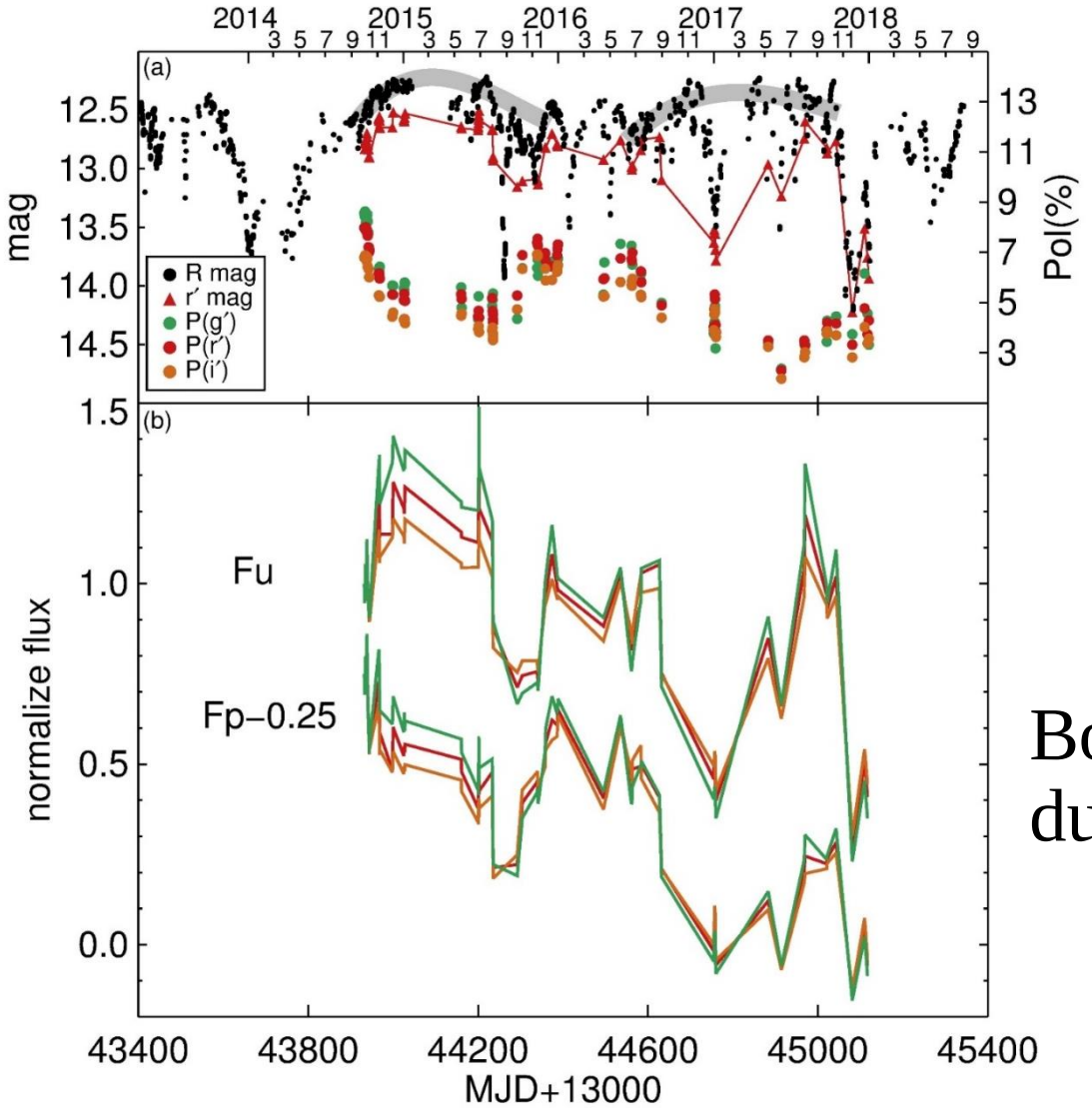

Polarization ~3%—9%

→ Slowly varying, inversely with system brightness

$$P_\lambda(\%) = \frac{F_\lambda^P}{F_\lambda^t} = \frac{F_\lambda^P}{F_\lambda^P + F_\lambda^u} = \frac{1}{1 + F_\lambda^u / F_\lambda^P}$$

Both F^u (star) and F^p (envelope) obscured by dust clumps

→ Wavelength dependence reversal at min

Polarimetry of YSOs

35 T Tauri stars, 5 HAEBE stars, and 3 UXors

- TTSs and HAEBEs by and large polarized
  ~ 90% T Tauri and 60% HAEBE with P <1.5%;
  Large P rare; no T Tauri stars > 3%
- In general, $P_{HAEBE} > P_{TT}$ because HAEBEs dusty and nebulous
- Polarization variability: TTSs ~59%; HAEBEs ~ 83%,
  Some vary in P%, some in PA, some both, and some in λ dep.

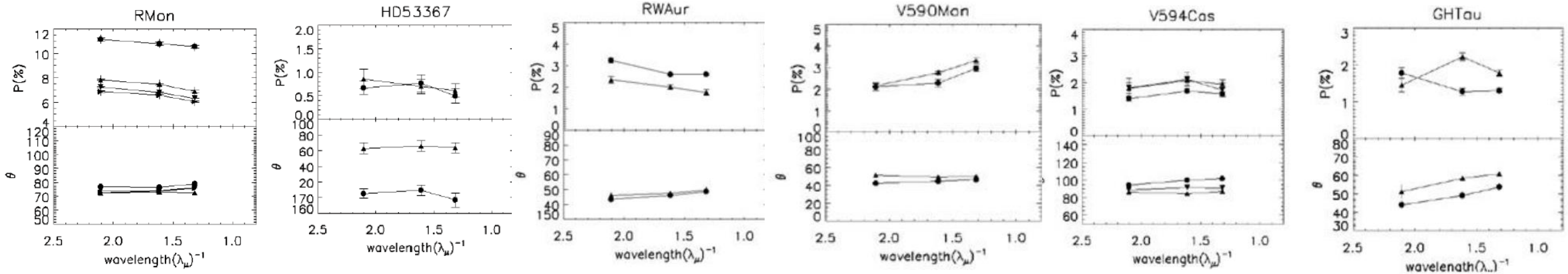

Imaging Polarimetry --- R Monocerotis

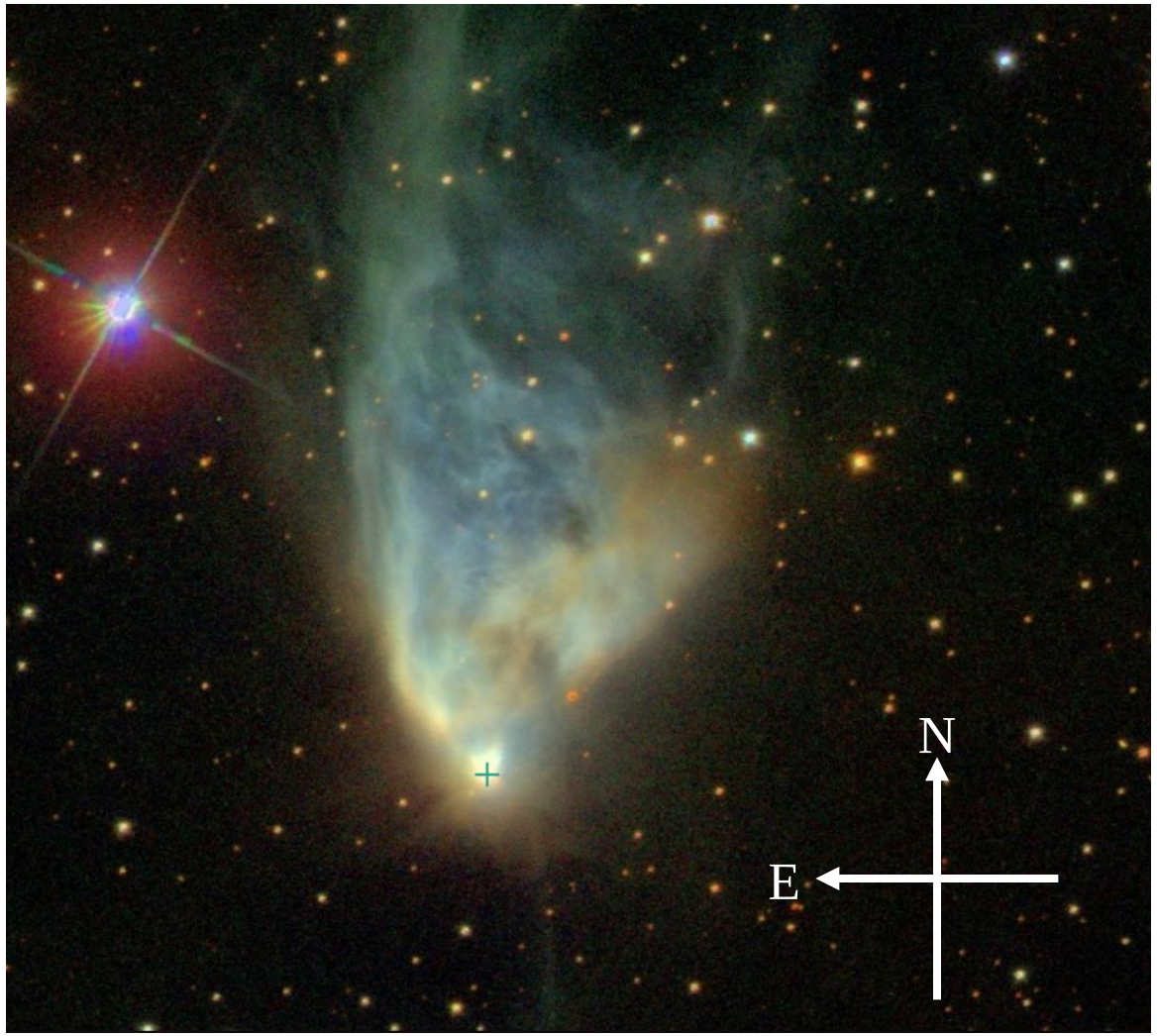

~4.5 arcmin

- Herbig Be @ ~760 pc
  (Herbig+60; Finkenzeller+84; Close+97)
- Associated with the variable reflection nebula NGC2261
  (Hubble 1916)
- Bipolar outflows: HH39
  (Canto+81; Jones & Herbig 82; Brugel+1984)
- A T Tauri companion @ 0.69” NW (~520 au) *(Close+97)*
- Inclination ~70 deg; north pole toward line of sight *(Close+97)*

P% anticorrelated with brightness

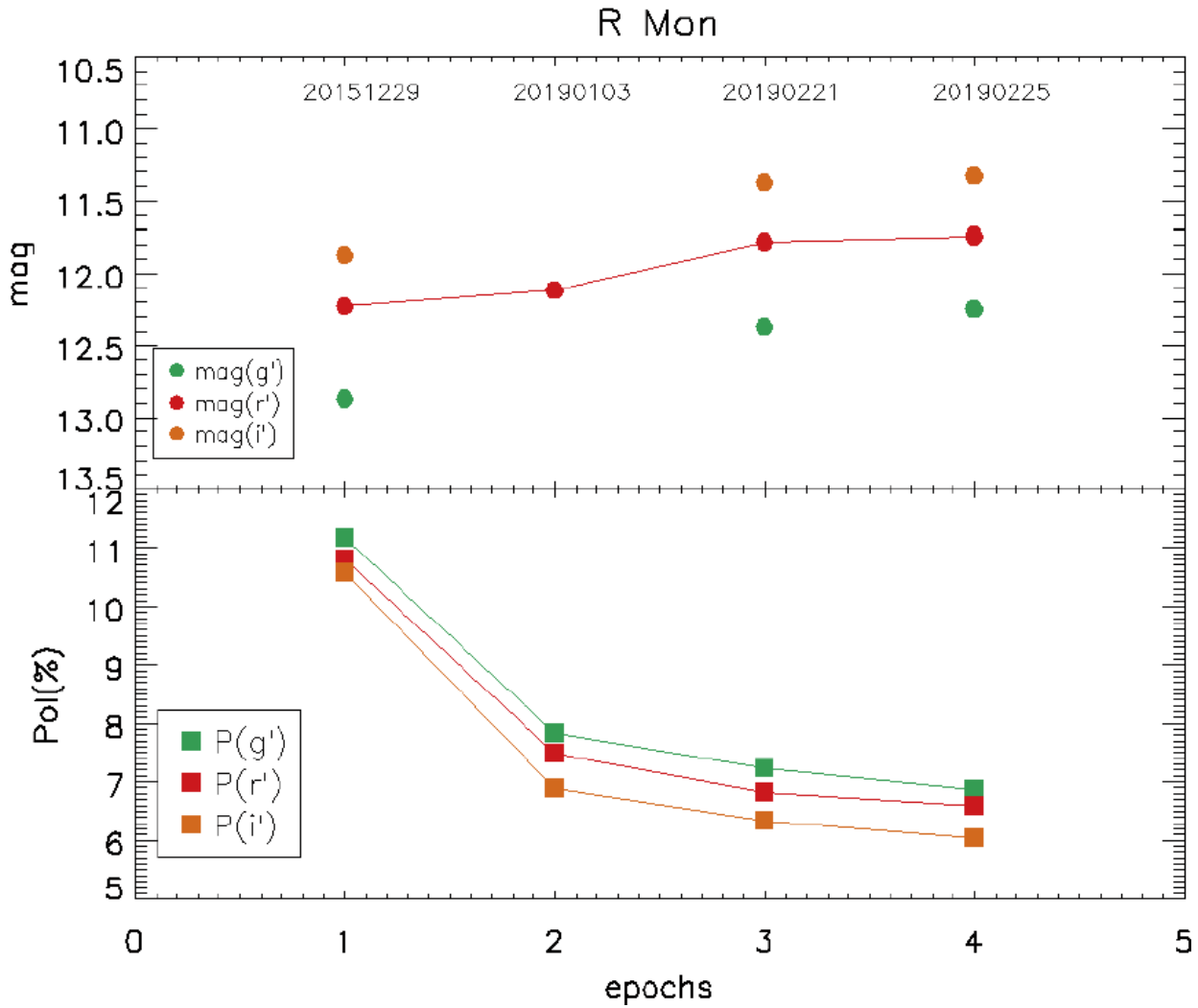

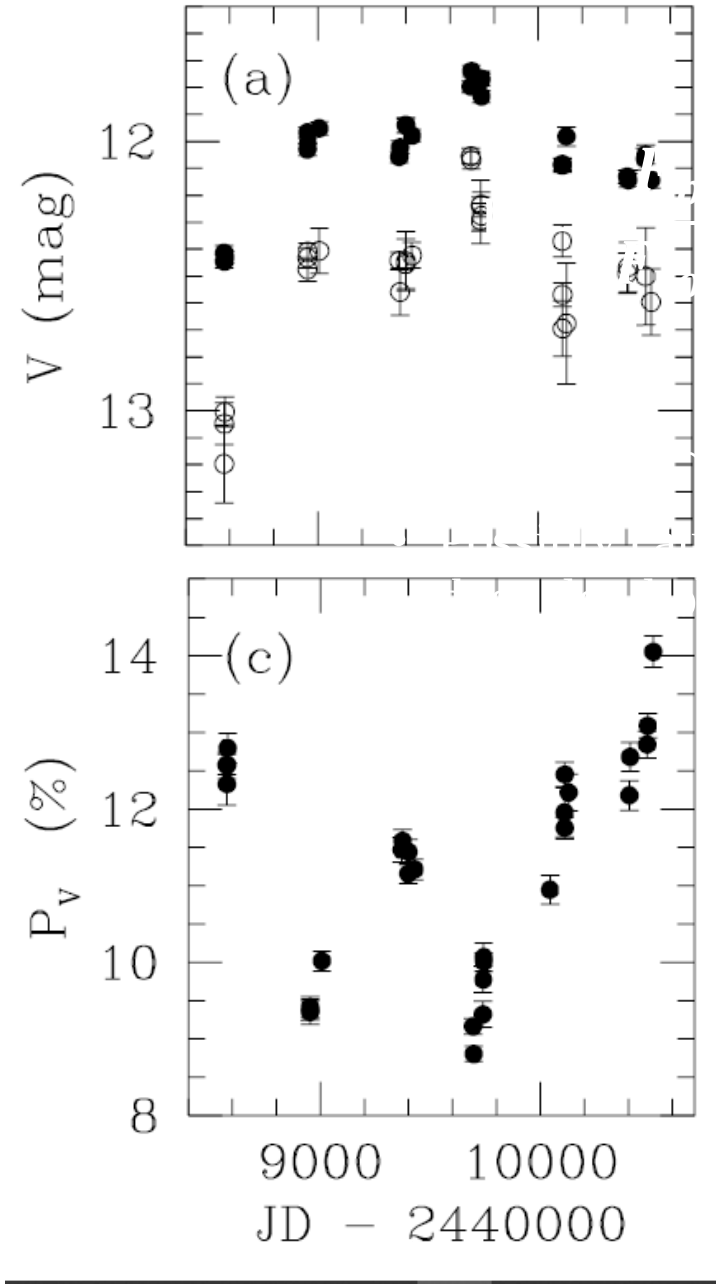

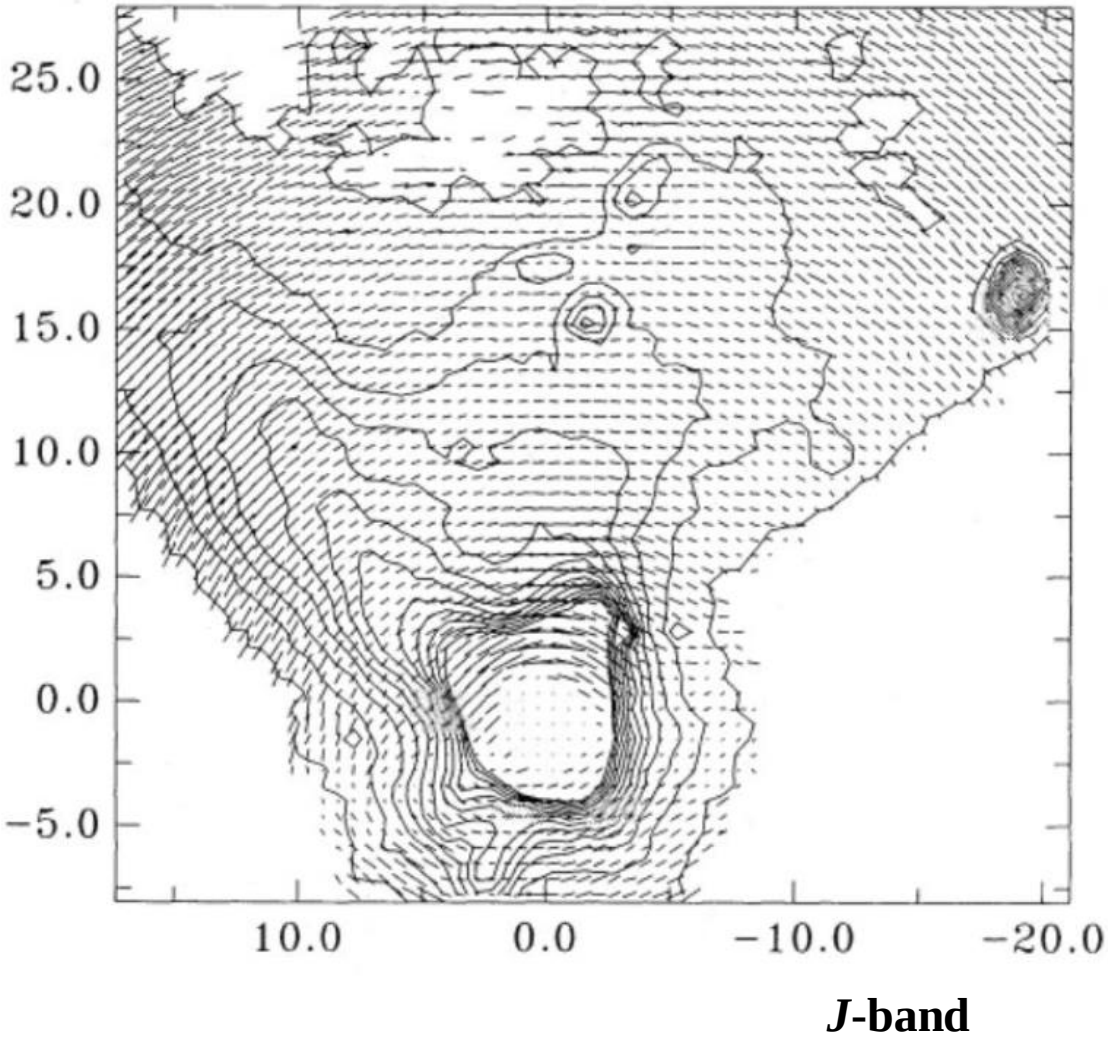

Minchin et al. 1991

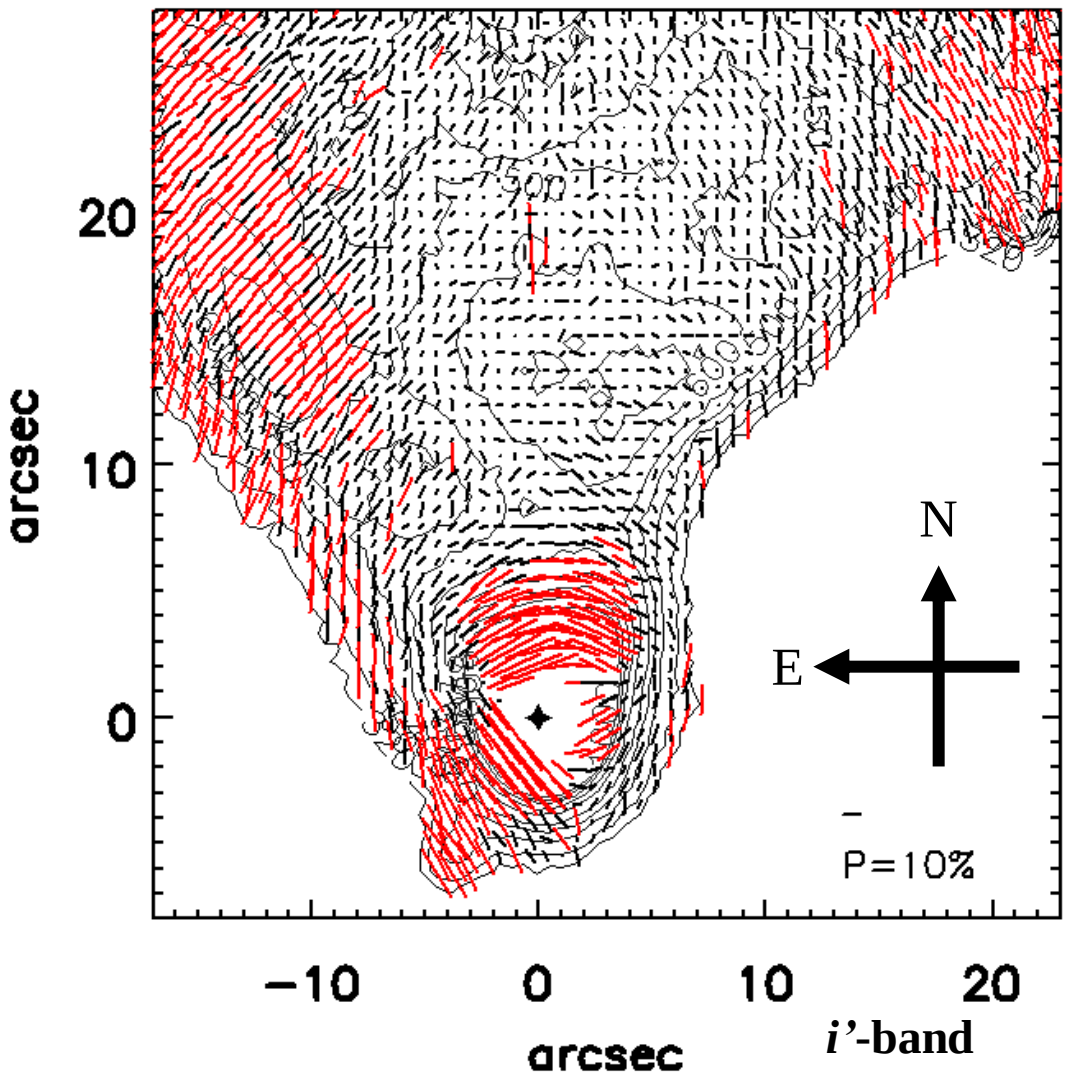

Huang+2019

Temporal Polarization Variation

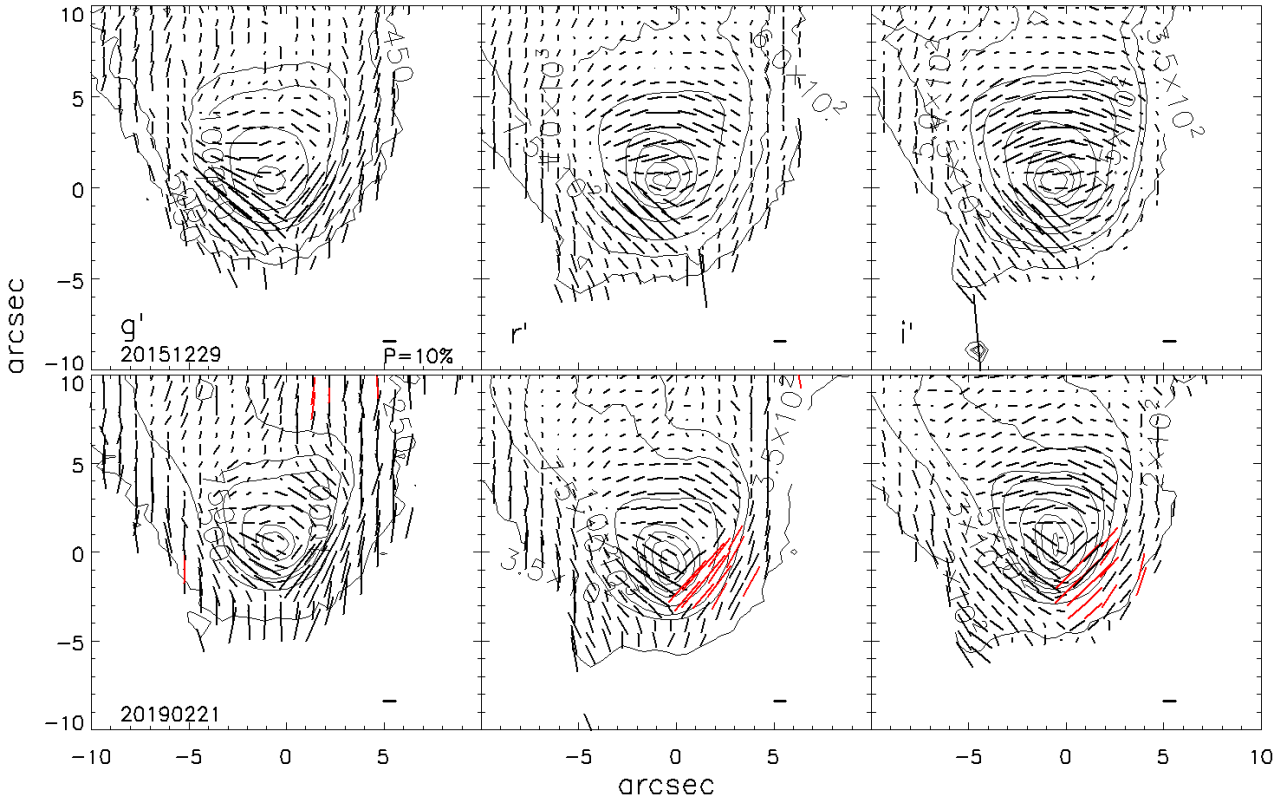

$P_{2019} > 20\%$ and $P_{2019} > 3P_{2015}$

Cannot be caused by the orbiting companion (~520 au NW)? → P~5000 yr *(Close et al. 1997)*, or by orbiting shells ~2”—3” (1500-2000 au) away

Possible mechanisms include shadowing by dust clumps close in to the star *(Matsumura et al. 1999)* or by emerging YSO jets *(Lightfoot 1989)*

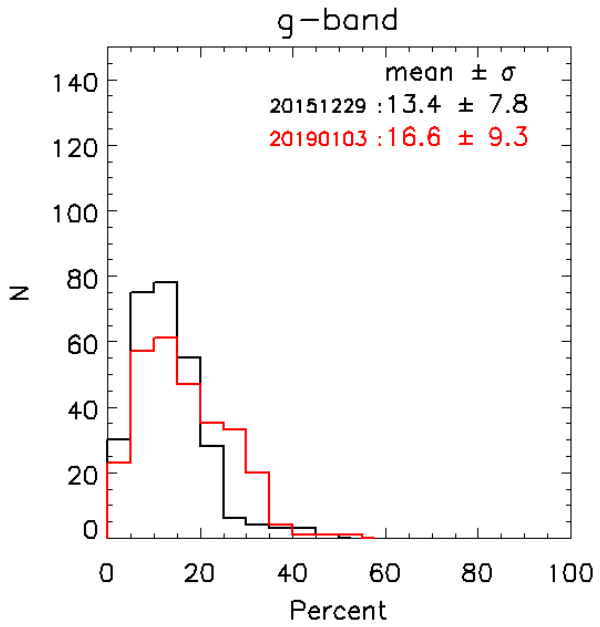
g−band
mean ± σ
20151229 :13.4 ± 7.8
20190103 :16.6 ± 9.3
N
Percent

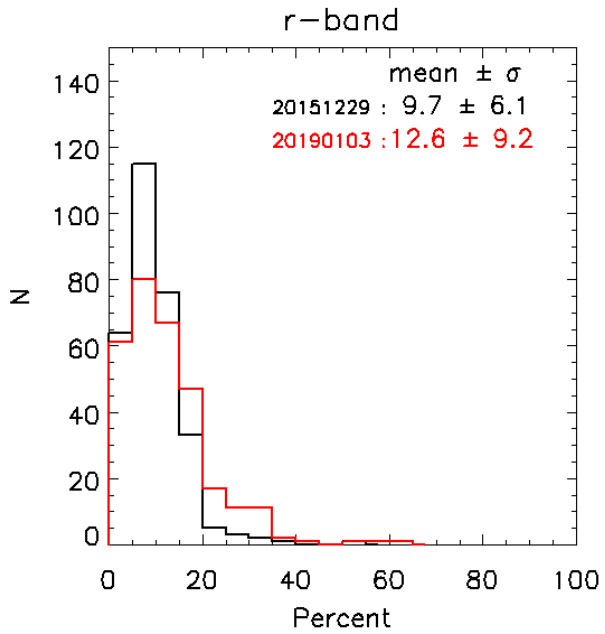
r−band
mean ± σ
20151229 : 9.7 ± 6.1
20190103 :12.6 ± 9.2
N
Percent

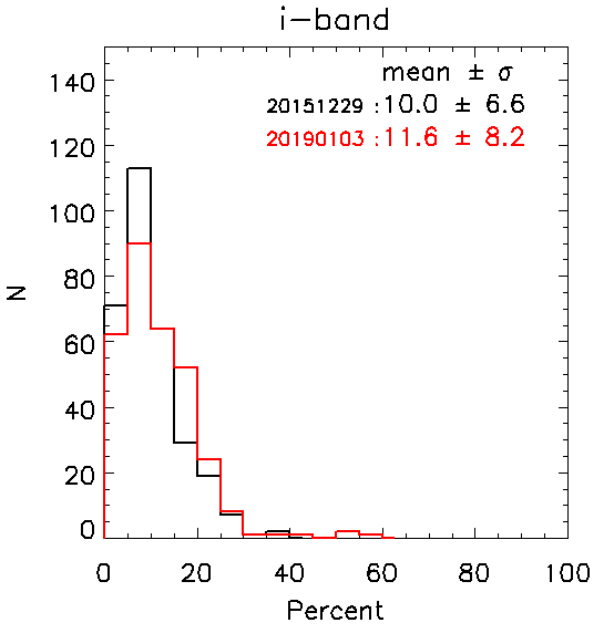
i−band
mean ± σ
20151229 :10.0 ± 6.6
20190103 :11.6 ± 8.2
N
Percent

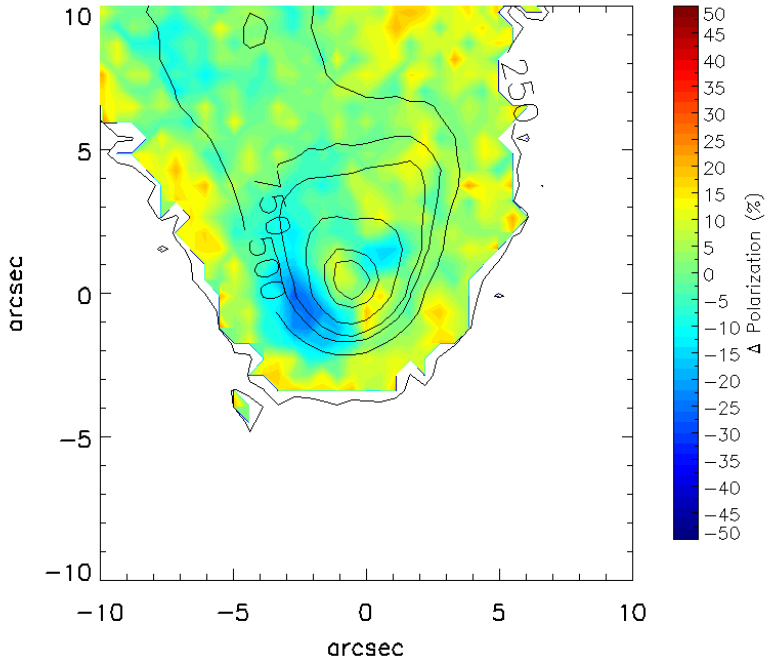
arcsec
Δ Polarization (%)

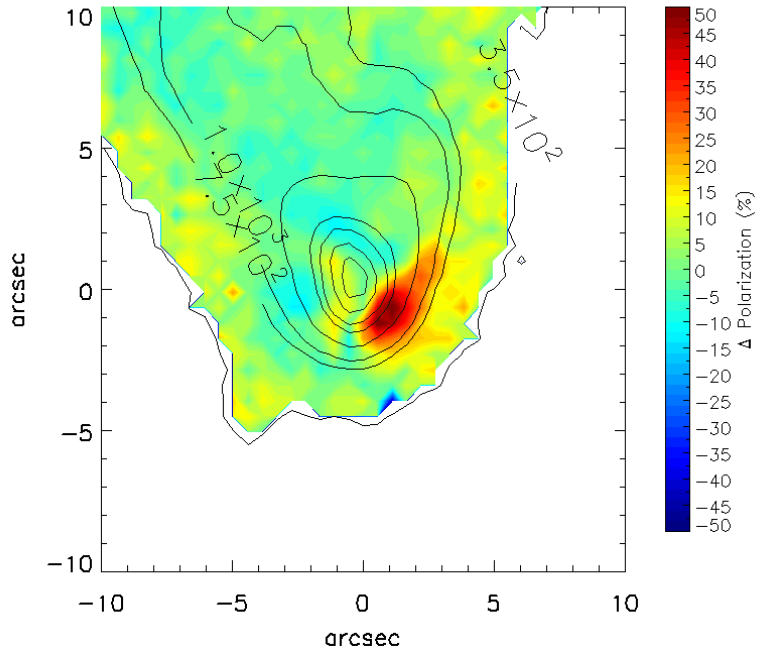
arcsec
Δ Polarization (%)

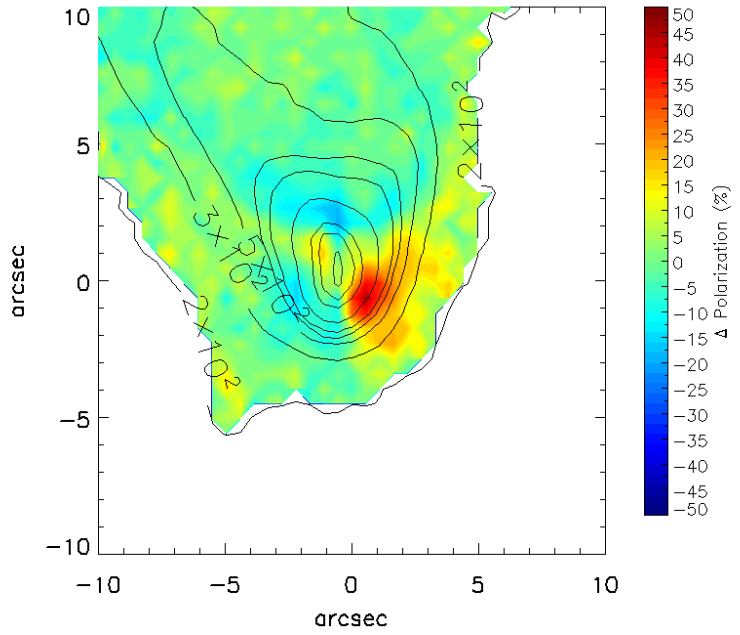
arcsec
Δ Polarization (%)

GJ3147 M7.5 V;10 pc
photometry/polarimetry campaign 2021 Nov 11 to 17

The same flare (a continuous function)

- ✓ by two telescopes (different sampling functions; discrete) → “true” profile
- ✓ at two bands → flare temperature
- ✓ Polarization on and off a flare → thermal/nonthermal cooling?

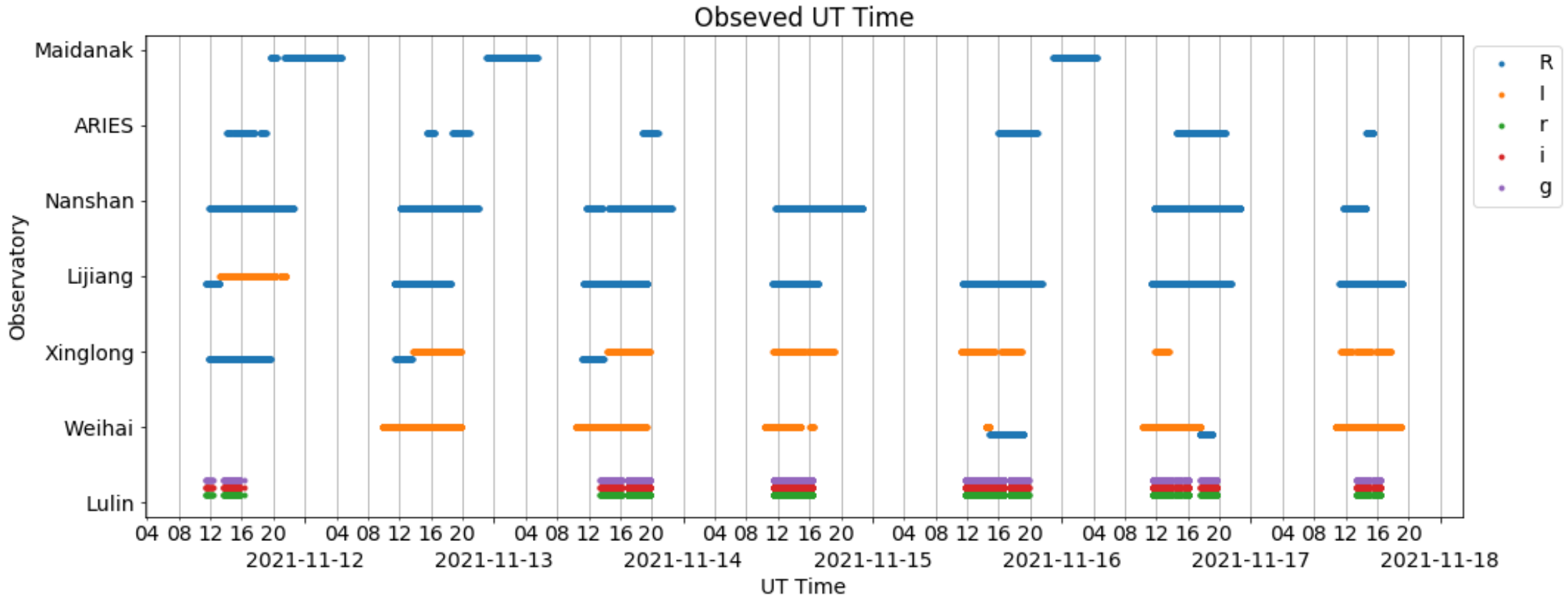

2021 Nov. 13

- 4 flare detected

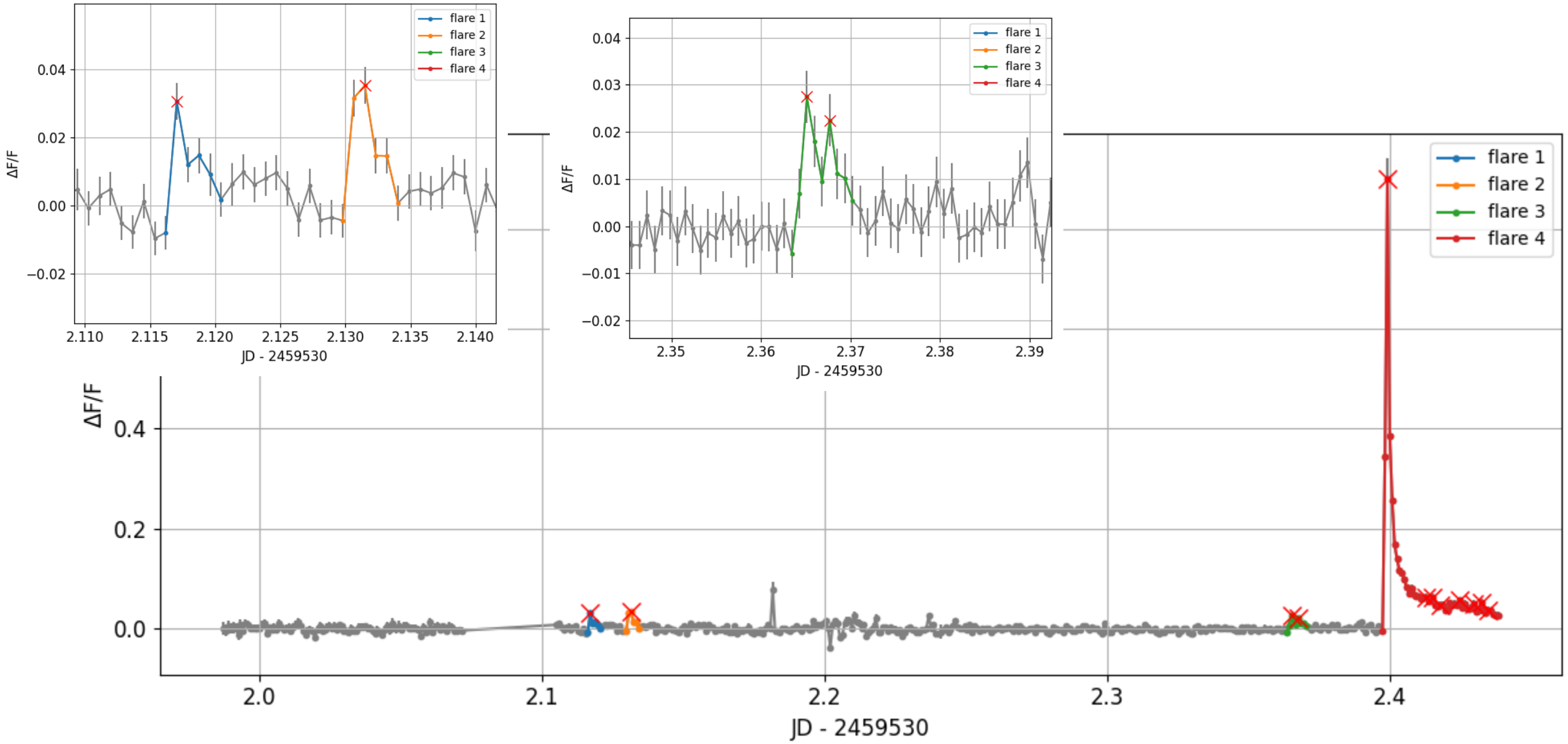

g

r

i

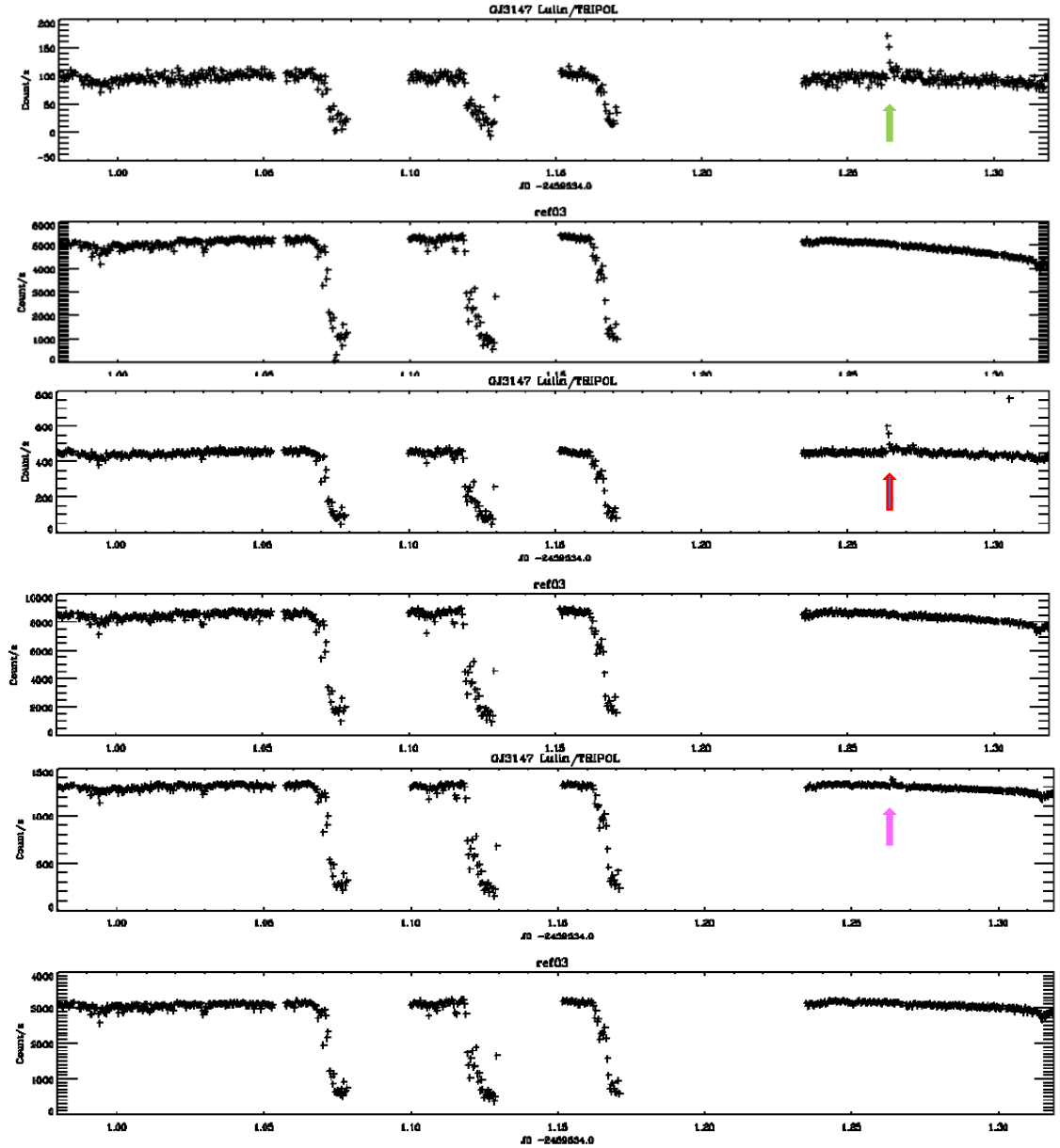

A major flare on 2021 Nov 16 detected with Lulin/TRIPOL (at g', r', i')

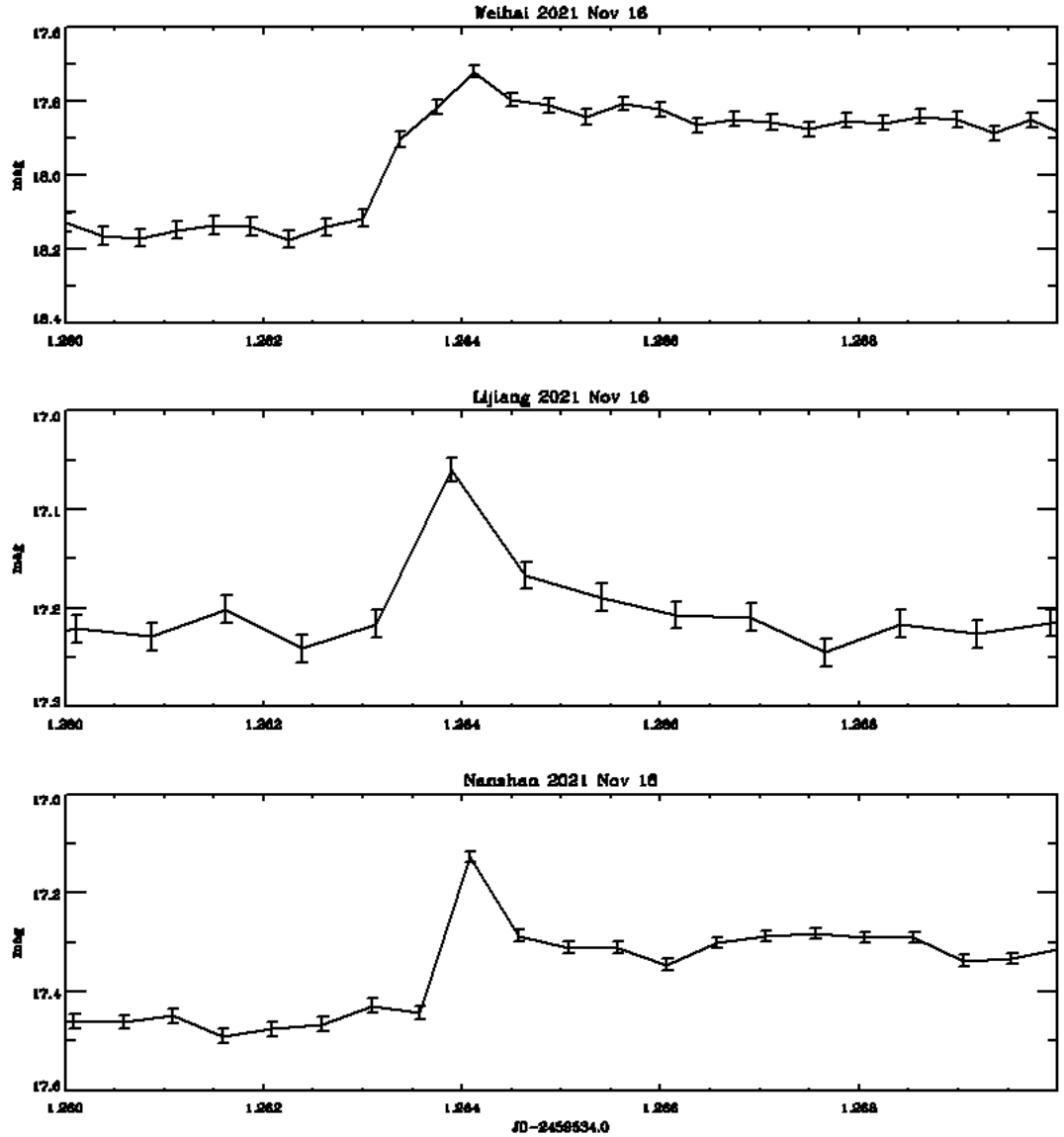

… and simultaneously by Weihai, Lijiang, and Nanshan (all at R)

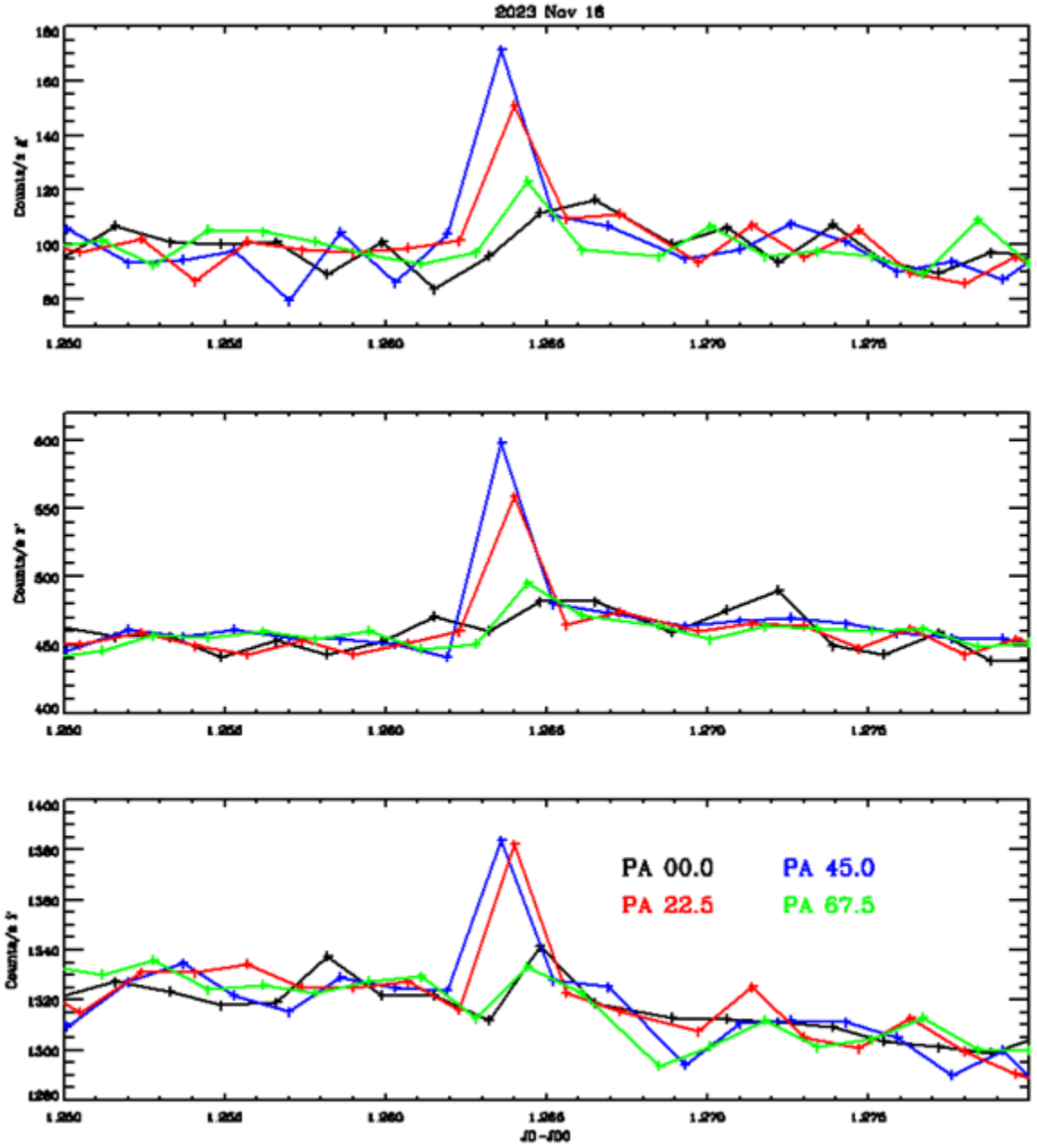

Polarimetry and photometry

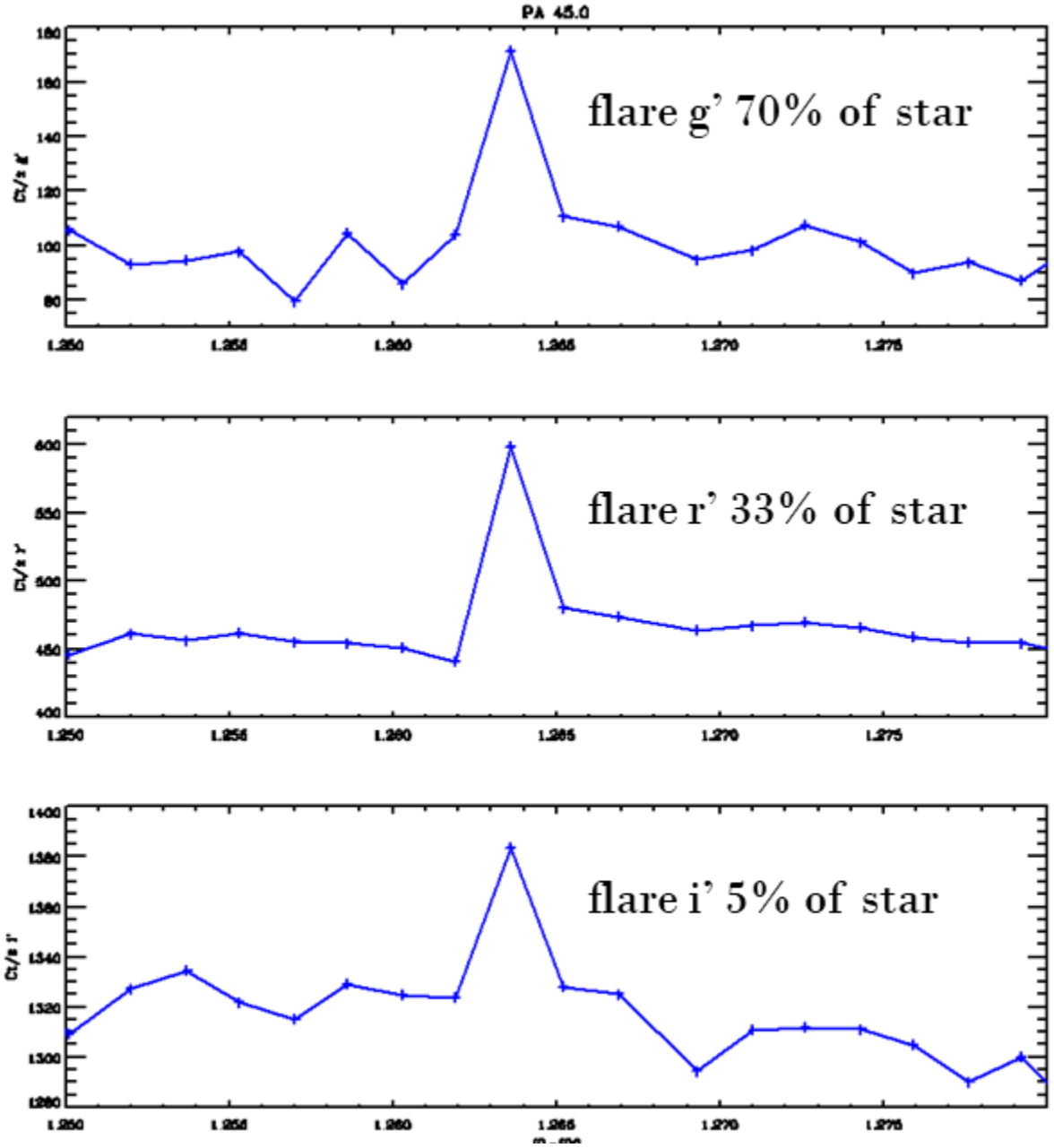

Photometry by the same sampling function

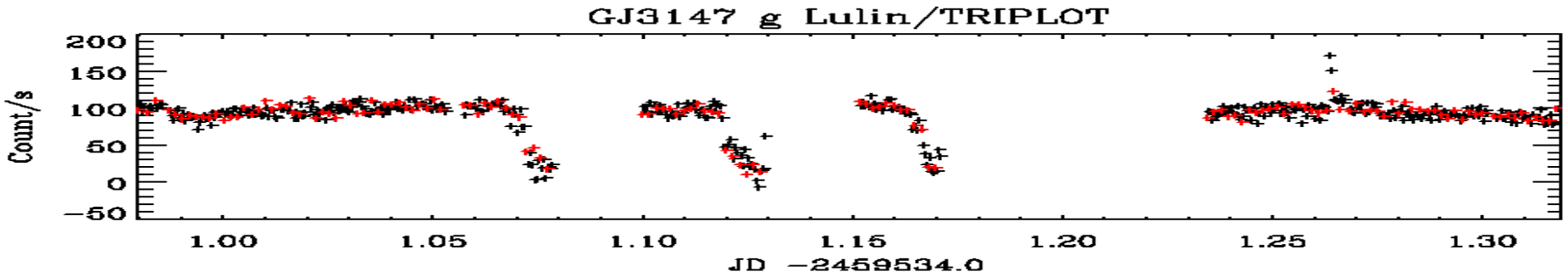

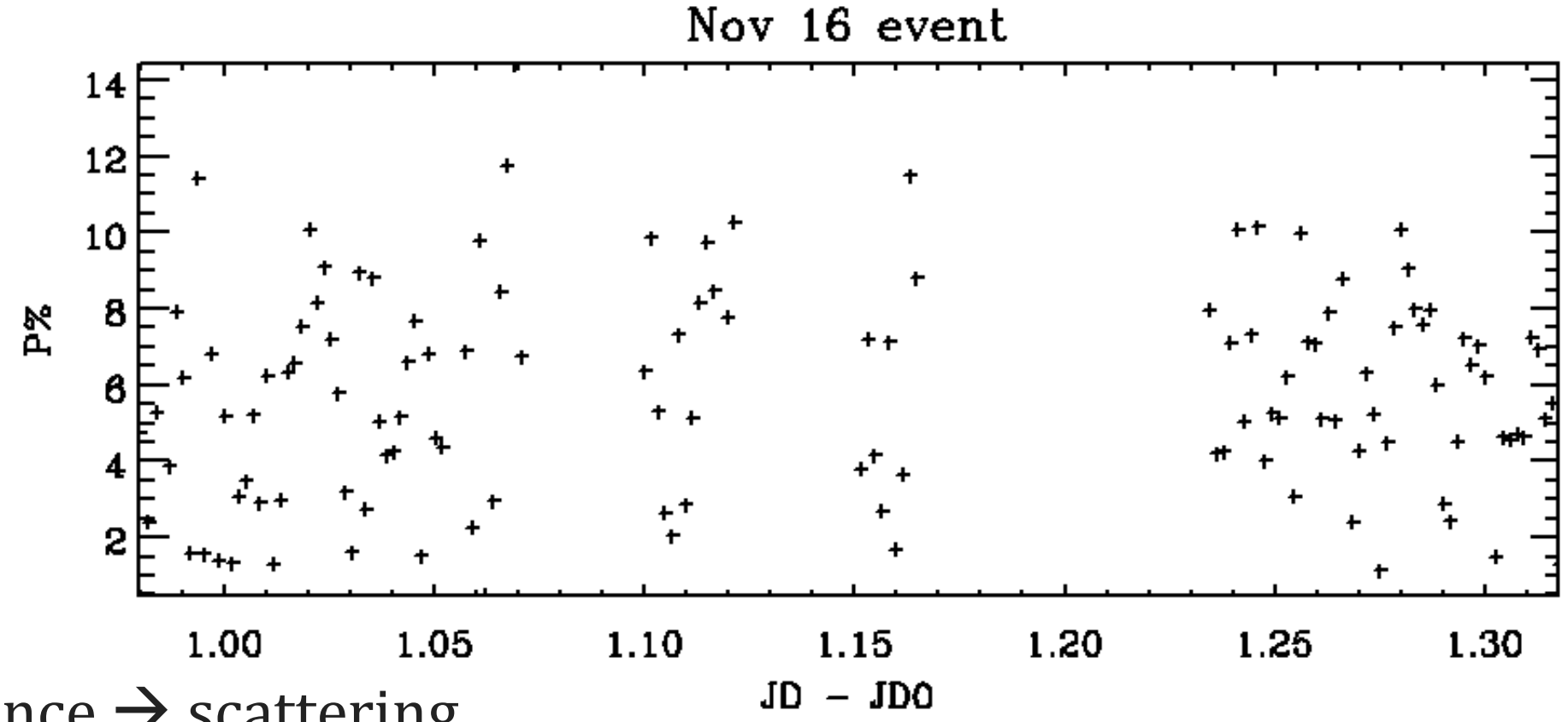

g': 5.8%
r': 2.0%
i': 0.5%
In quiescence → scattering

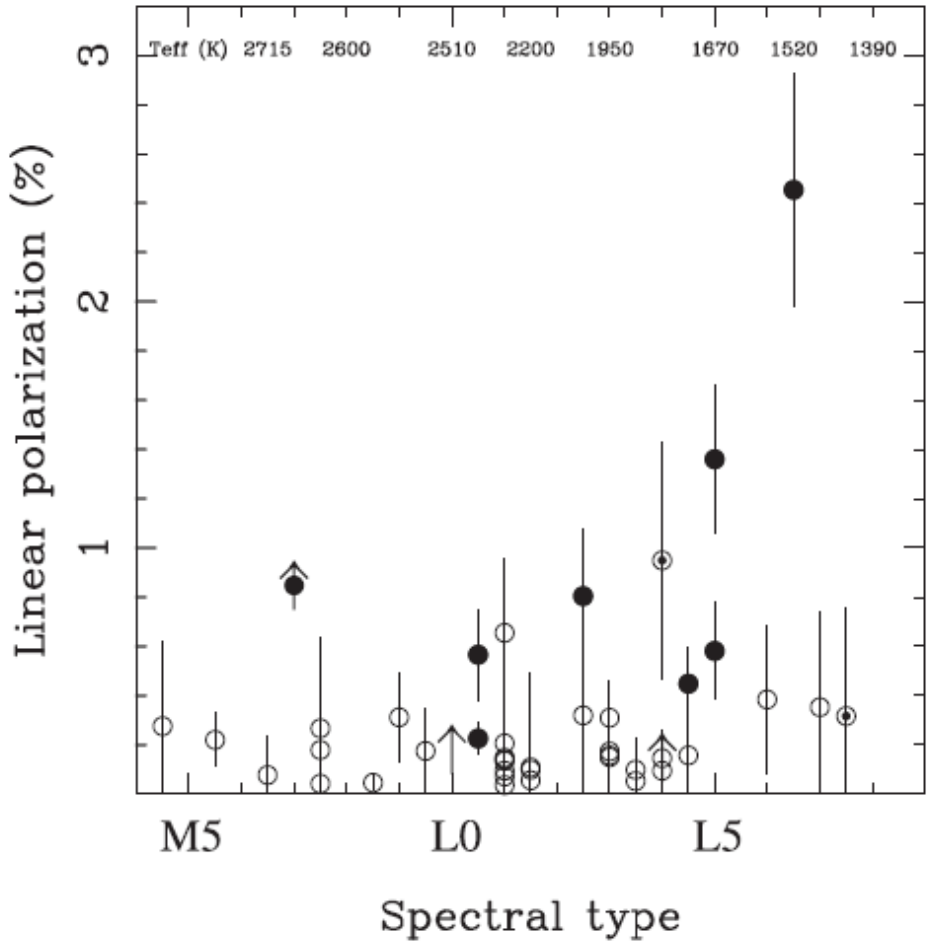

FIG. 2.—*I*-band linear polarization of our target sample against spectral type. Likely polarized sources are plotted as filled circles. Arrows denote lower limits ($P \geq |Q/I|$), and open circles stand for nondetections. The mean values of J2158−15 and J2252−17 are plotted as circled dots. The $T_{\rm eff}$− spectral type calibrations of Dahn et al. (2002; late-M) and Vrba et al. (2004; L types) are given on the top of the figure. The uncertainty in spectral type is half a subclass.

Zapatero Osorio+05

Polarization of ultracool dwarfs
($T = 1300 - 2700$ K; late-M, L to T spT)

P% generally $\lesssim 1 - 2$%, but the cooler the stronger

Scattering off

✓ Inhomogeneous medium (clouds)

✓ Fast rotation → oblate atmosphere

Conclusions

- The compact, robust, and economic simultaneous 3-channel imaging photometer TRIPOL is useful for a small telescope.
  - ✓GM Cep has a measured polarization of 3% to 9% at g'r'i', which correlates with brightness and with colors. The star has a clumpy disk likely associated with planetesimal formation.
  - ✓Herbig Ae/Be stars generally are more polarized, and with greater variability, than T Tauri stars, due to copious CS dust and gas.
- Polarimetry (and its variability) is an added (powerful) tool to diagnose the circumstellar environments of YSOs, and energetic events (AGNs, stellar flares, etc.)
- OIR spectro-polarimetric instruments are highly desirable on mid-sized or large telescopes, e.g., 司空望遠鏡、7-dimensional Telescope (7DT)